Miscellaneous Paper HL-94-7
October 1994

US Army Corps
of Engineers
Waterways Experiment
Station

Application of a Two-Dimensional Model of Hydrodynamics to San Timoteo Creek Flood-Control Channel, California

by Richard L. Stockstill

Approved For Public Release; Distribution Is Unlimited

Prepared for U.S. Army Engineer District, Los Angeles

The contents of this report are not to be used for advertising, publication, or promotional purposes. Citation of trade names does not constitute an official endorsement or approval of the use of such commercial products.

PRINTED ON RECYCLED PAPER

Miscellaneous Paper HL-94-7
October 1994

Application of a Two-Dimensional Model of Hydrodynamics to San Timoteo Creek Flood-Control Channel, California

by Richard L. Stockstill

U.S. Army Corps of Engineers
Waterways Experiment Station
3909 Halls Ferry Road
Vicksburg, MS 39180-6199

Final report

Approved for public release; distribution is unlimited

Prepared for U.S. Army Engineer District, Los Angeles
Los Angeles, CA 90053-2325

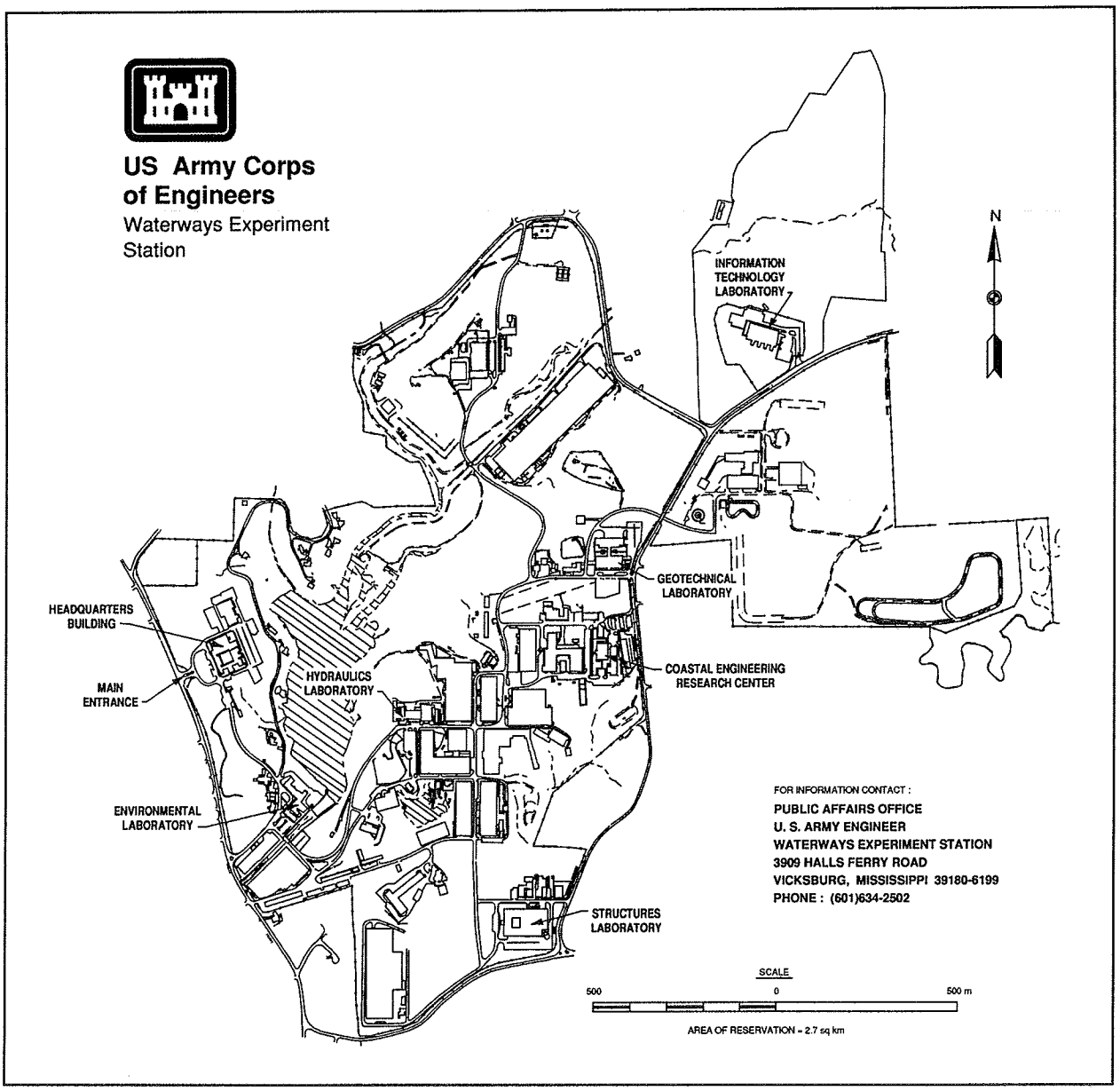

Waterways Experiment Station Cataloging-in-Publication Data

Stockstill, Richard L.
Application of a two-dimensional model of hydrodynamics to San Timoteo Creek flood-control channel, California / by Richard L. Stockstill ; prepared for U.S. Army Engineer District, Los Angeles.
49 p. : ill. ; 28 cm. — (Miscellaneous paper ; HL-94-7)
Includes bibliographic references.
1. Flood control — California — San Bernardino County. 2. San Timoteo Creek (Calif.) — Channelization. 3. River engineering — California — San Timoteo Creek. 4. Stream channelization — California — Riverside County. I. United States. Army. Corps of Engineers. Los Angeles District. II. U.S. Army Engineer Waterways Experiment Station. III. Hydraulics Laboratory (U.S.) IV. Title. V. Series: Miscellaneous paper (U.S. Army Engineer Waterways Experiment Station) ; HL-94-7.
TA7 W34m no.HL-94-7

Contents

Preface iv

Conversion Factors, Non-SI to SI Units of Measurement v

1-Introduction 1

Background 1
Purpose 2
Approach 2

2-Model Description 3

Governing Equations 3
Assumptions and Limitations 3

3-Model Applications 4

Geometry and Computational Mesh 4
Boundary Conditions 5
Model Parameters 5

4-Results 7

Design Discharge, 19,000 cfs 7
Initial tests (n = 0.014) 7
Decreased roughness (n = 0.012) 11
12,000-cfs Discharge 12

5-Summary and Conclusions 14

References 15

Tables 1-5

Plates 1-12

Appendix A: The Hydrodynamic Model: HIVEL2D A1

SF 298

Preface

The two-dimensional numerical modeling of the flow conditions in the proposed San Timoteo Channel was performed for the U.S. Army Engineer District, Los Angeles (SPL). The study was authorized by the U.S. Army Engineer Division, South Pacific, on 26 August 1993. SPL personnel involved in this study were Mr. Algis Bliudzius and Ms. Wendy Gist under the supervision of Mr. Brian Tracy, Chief of the Hydraulics Section.

The study was conducted in the Hydraulics Laboratory of the U.S. Army Engineer Waterways Experiment Station (WES) during the period December 1993 to April 1994 under the direction of Messrs. F. A. Herrmann, Jr., Director of the Hydraulics Laboratory; R. A. Sager, Assistant Director of the Hydraulics Laboratory; and G. A. Pickering, Chief of the Hydraulic Structures Division, Hydraulics Laboratory.

This work was performed by Messrs. Richard L. Stockstill and Mikel W. Ott under the supervision of Mr. John F. George, Chief, Locks and Conduits Branch, Hydraulic Structures Division. Technical assistance in the form of consultation and peer review was provided by Dr. R. C. Berger, Estuaries Division, Hydraulics Laboratory. The report was prepared by Mr. Stockstill.

At the time of publication of this report, Director of WES was Dr. Robert W. Whalin. Commander was COL Bruce K. Howard, EN.

The contents of this report are not to be used for advertising, publication, or promotional purposes. Citation of trade names does not constitute an official endorsement or approval of the use of such commercial products.

Conversion Factors, Non-SI to SI Units of Measurement

Non-SI units of measurement used in this report can be converted to SI units as follows:

Multiply	By	To Obtain
cubic feet	0.02831685	cubic meters
degrees (angle)	0.01745329	radians
feet	0.3048	meters

1 Introduction

Background

The San Timoteo Creek is a tributary of the Santa Ana River and drains portions of San Bernardino and Riverside Counties (Figure 1). The existing creek has the capacity to protect the surrounding community from approximately a 20-year-frequency flood (U.S. Army Engineer District, Los Angeles, 1993). The recommended plan would provide a 100-year level of protection (19,000 cfs).[1]

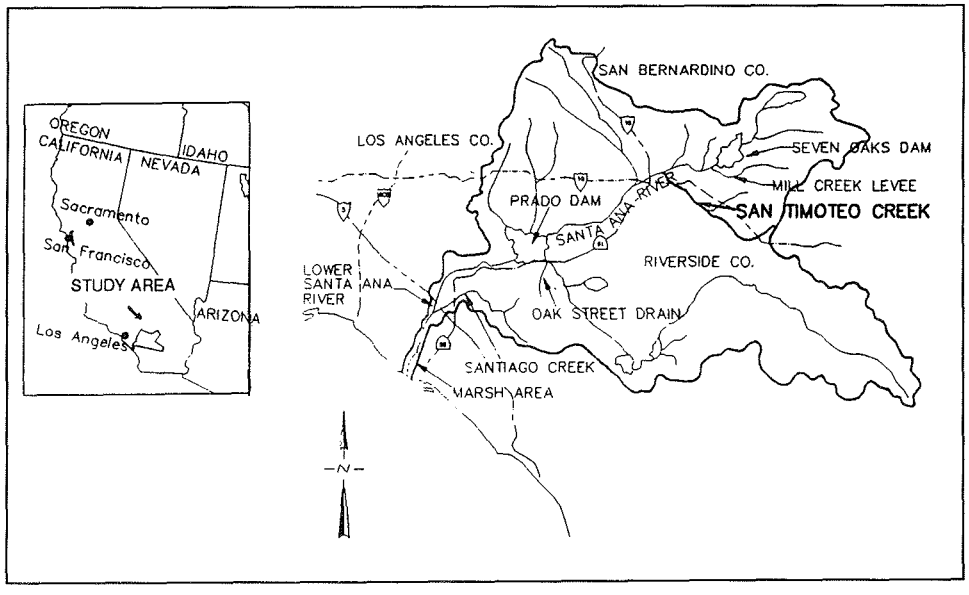

Figure 1. Vicinity and location maps

The proposed design within the reach studied includes a sediment basin (the last of a series of basins for the project), a concrete weir followed by a chute having converging sidewalls, a compound horizontal curve consisting of spirals between a circular curve and the upstream and downstream tangents

[1] A table of factors for converting non-SI units of measurement to SI units is found on page v.

with a banked invert, and a bridge pier associated with the San Timoteo Canyon Road. The modeled reach extended from basin sta 5+00 to channel sta 280+00, resulting in a total simulated channel length of 2,396.94 ft. Geometrical details of the proposed channel design are shown in the plan view provided in Plate 1.

Purpose

This investigation was initiated because there was concern as to the adequacy of a one-dimensional analysis of the flow conditions within the channel chute. There was a question as to whether computing cross-sectional averaged flow variables provided a sufficiently accurate estimate of flow depths within the geometrically complex chute. It was known that the supercritical flow in the chute would produce oblique standing waves. These waves do not present a problem as long as the channel walls are of sufficient height. However, the flow conditions in the upper end of the channel are further complicated by the fact that the chute is followed by a channel curve, followed by the San Timoteo Canyon Road bridge. A two-dimensional analysis was deemed necessary to evaluate the chute's influence on the flow conditions in the curve and the curve's impact on the flow conditions at the bridge.

Approach

The two-dimensional, depth-averaged flow model, HIVEL2D, was used to simulate the flows in the high-velocity channel. This model was chosen because of its ability to simulate supercritical flow and capture shocks such as oblique standing waves.

2 Model Description

Governing Equations

HIVEL2D (Stockstill and Berger 1994) solves the depth-averaged unsteady shallow-water equations implicitly using finite elements. The shallow-water equations are the result of vertical integration of the equations of mass and momentum conservation for incompressible flow assuming hydrostatic pressure distribution. The dependent variables of the two-dimensional fluid motion are defined by the flow depth and the x-direction and y-direction components of unit discharge. These variables are functions of the spatial Cartesian coordinates x and y and time. A brief description of the finite element model is provided in Appendix A.

Assumptions and Limitations

An important (and standard) assumption made in the derivation of the governing equations is that vertical accelerations are negligible when compared to the horizontal accelerations and the acceleration due to gravity. This assumes that the pressure distribution is hydrostatic. The hydrostatic pressure assumption is generally applicable to high-velocity channels; however, certain limited areas of the flow field are decidedly nonhydrostatic. One must resort to engineering judgment to assess the ramifications of this difference, noting that hydrostatic models overestimate the speed of short wavelengths.

Another significant assumption is that the invert slope is geometrically mild (less than about 0.02), though it may be hydraulically steep, producing supercritical flow. This is a reasonable assumption for most high-velocity channels. However, the flow speed in long channel reaches with a favorable slope greater than about 0.05 will tend to be overestimated and the flow depth will tend to be underestimated, whereas adverse steep slopes will tend to overestimate the flow depth and underestimate the flow speed. A general discussion of the assumptions associated with the shallow-water equations is presented in Berger and Stockstill (1994).

3 Model Applications

Application of the model to the proposed channel design requires the construction of a numerical model computational mesh to represent the design's geometry and the specification of boundary conditions and model parameters.

Geometry and Computational Mesh

The reach of the San Timoteo Creek channel modeled in this study was from basin sta 5+00 to 0+20 and from channel sta 299+16.94 to 280+00, a total length of 2,396.94 ft. The subcritical flow in the sediment basin at the upper end is controlled by the concrete weir, which begins the concrete-lined high-velocity channel. The upstream face of the weir is a 1V on 2H slope. The weir crest, which is immediately followed by a 940-ft converging sidewall chute, is 20 ft long in the direction of flow. The chute was designed to transition from the 338-ft-wide sediment basin to the 86-ft-wide high-velocity channel. A channel bend is located 83.35 ft downstream of the chute end. The bend was designed with spiral curves and a banked invert. The San Timoteo Canyon Road crosses the channel downstream of the bend. One pier for this bridge is located within the channel, near the channel center line. Plate 1 shows a plan view of the modeled reach.

The width of the flow domain within the sediment basin is dependent on the water-surface elevation in this vicinity because the channel sidewalls are sloping. Therefore, the numerical model computational mesh of the sediment basin was different for the two discharges simulated. Initial numerical tests were conducted to determine an adequate top bank elevation to use for the domain limit. By trial, a top bank of elevation 1316.0[1] was found appropriate for modeling a discharge of 19,000 cfs. Representing the basin flow using a fixed grid was deemed adequate because the flow in this region is subcritical. Fixed grid boundary conditions are sufficient for simulation of steady subcritical flow in channels having sloping sidewall boundaries.

---

[1] All elevations (el) cited herein are in feet referenced to the National Geodetic Vertical Datum (NGVD).

The San Timoteo Canyon Road bridge pier presently has a semicircular nose and tail. The pier was modeled with a triangular nose and tail. Significantly more grid refinement would be needed to simulate a semicircular nose and tail and was not deemed necessary for this study. Proposed channel modifications include the addition of a debris nose on this pier. A sloping debris nose cannot be accurately modeled with a depth-averaged model; therefore, only the existing pier configuration was simulated in this study.

The numerical model computational mesh is shown in Plate 2. The mesh consisted of 945 nodes and 918 elements. Grid resolution was more refined in the vicinity of sidewall boundary alignment changes and at all grade breaks.

Boundary Conditions

This study included the simulation of two discharges, the design discharge of 19,000 cfs and a lesser discharge of 12,000 cfs. The inflow boundary located in the sediment basin was subcritical and therefore required two boundary conditions. The x- and y-direction components of unit discharge were specified for the inflow boundary conditions. These unit discharges were computed assuming a constant velocity over the inflow boundary cross section. A water-surface elevation at the inflow boundary was assumed, then the inflow velocity was computed as the discharge divided by the flow area. The unit discharges were calculated as the product of the flow depth at each inflow node times the computed velocity. These unit discharges were further resolved into x- and y-components normal to the inflow boundary. The outflow boundary was supercritical and therefore required no boundary conditions.

Model Parameters

Model and flow parameters used in the initial simulation are provided in the following tabulation, where α is the temporal differencing weight ($\alpha = 1$ is first-order and $\alpha = 1.5$ is second-order backward differencing); β_{SM} and β_{SH} are the Petrov-Galerkin parameters for smooth flow and for shocks, respectively; C_{SM} and C_{SH} are the coefficients used in determination of eddy viscosity; and g is acceleration due to gravity. Descriptions of these conditions are presented in Appendix A.

Model Condition	Value
α	1.0
β_{SM}, β_{SH}	0.1, 0.5
C_{SM}, C_{SH}	0.1, 0.5
g	32.2 ft/sec^2

Because a steady-state solution was sought, the temporal difference order was irrelevant. Therefore, a first-order temporal differencing was used in all simulation runs.

4 Results

As stated previously, this study included the simulation of two discharges, the design discharge of 19,000 cfs and a lesser discharge of 12,000 cfs. This 12,000-cfs discharge was selected for testing because a one-dimensional analysis conducted by the U.S. Army Engineer District, Los Angeles, found that the 12,000-cfs discharge actually resulted in larger Froude numbers in the channel chute. It was felt that these larger Froude numbers might be accompanied by higher standing waves at a particular station than those produced by the design discharge (19,000 cfs).

The prototype flow geometry and boundary roughness for the concrete channel reach will most likely result in a Manning's n value of approximately 0.014. The concrete reach of channel extends from the toe of the upstream face of the weir (basin sta 0+44 at center line) downstream to the end of the modeled reach (sta 280+00). However, an envelope of possible hydraulic conditions was established by also performing simulations of the flow conditions resulting from a very smooth boundary by using an n value of 0.012. All simulations used an n of 0.030 for the sediment basin, which has riprapped side slopes and a natural bed.

The sensitivity of simulation results to the choice of model parameters and mesh refinement was determined. This sensitivity was established by changing one condition per run and then comparing the results with previous runs to assess the condition's impact on simulation results.

Design Discharge, 19,000 cfs

Initial tests (n = 0.014)

Water-surface profiles resulting from a discharge of 19,000 cfs and an n value of 0.014 are presented in Plate 3 and in tabular form in Table 1. The profiles illustrate the variation in the depth of flow at the sidewalls resulting from supercritical flow in the channel chute. A significant setup is noted in the channel bend. It is interesting to note the rise in the water-surface elevation in the basin as the flow approaching the structure decelerates. Of course the total energy grade line decreases in the direction of flow, but due to the

gradual expansion of the basin, the velocity head reduction is greater than the loss of total head. It is clearly shown in the profile that sufficient clearance is provided through the San Timoteo Canyon Road bridge. The significant runup on the upstream face of the pier is more of a model artifact than what would actually occur. Vertical accelerations immediately upstream of the pier nose are of such magnitude that the hydrostatic assumption is not valid.

A hydrostatic model provides a poor estimate of this sudden runup. To illustrate this point, a first approximation of the magnitude of these accelerations results in the conclusion that this pier nose runup is a violation of the hydrostatic assumption and that the runup is overestimated. A first approximation of the magnitude of these accelerations is obtained by applying the kinematic boundary condition to the water surface:

$$w_s = \frac{dh}{dt} = \frac{\partial h}{\partial t} + |V| \frac{\partial h}{\partial s} \tag{1}$$

where

w_s = vertical component of velocity at the water surface

h = flow depth

t = time

s = stream direction

and

$$|V| = (u^2 + v^2)^{1/2}$$

where u and v are the x- and y-direction components of velocity, respectively. The vertical acceleration a_z is:

$$a_z = \frac{dw}{dt} = \frac{\partial w}{\partial t} + |V| \frac{\partial w}{\partial s} + w \frac{\partial w}{\partial z} \tag{2}$$

Neglecting the last term and applying to steady flow,

$$w_s = |V| \frac{\partial h}{\partial s} \tag{3}$$

and

$$a_z = |V| \frac{\partial w}{\partial s} = |V| \frac{\partial}{\partial s} \left[|V| \frac{\partial h}{\partial s} \right] \tag{4}$$

Using difference approximations of the results of a simulation of 19,000 cfs and an n value of 0.014, the ratio of a_z/g at the pier nose was calculated to be 9.7. This definitely violates the hydrostatic assumption, i.e., that the vertical accelerations are negligible when compared to gravity (Appendix A). Pressures at the pier nose in the actual system (prototype) will be greater than hydrostatic, which will act to suppress the water-surface rise. Determination of what the water-surface elevation will be in the prototype is difficult. However, it will be significantly less than that calculated assuming a hydrostatic pressure distribution.

To illustrate that the hydrostatic assumption is appropriate elsewhere in the flow field, the vertical acceleration was approximated in the area of the oblique standing wave initiated at the pier nose (sta 282+10, 10 ft right of center line). The vertical acceleration in this vicinity, relative to gravity, was calculated to be 0.4. Although this is not insignificant, it shows that the hydrostatic assumption is reasonable even in areas where the flow is extremely rough.

Depth contours for a discharge of 19,000 cfs and an n value of 0.014 are presented in Figure 2. Depth contours within the chute are shown in Figure 3. The contours illustrate the oblique standing waves resulting from the converging sidewalls. Vertically exaggerated water-surface mesh plots (Plates 4 and 5) show the variation in depths and the superelevation in the channel bend. Depth contours in the vicinity of the bridge are provided in Figure 4.

At this point in the study, there was interest in the effect of the oscillations of the computed depths at the sidewalls in the vicinity of the crest on the results downstream, particularly if these oscillations were a numerical rather than a physical phenomenon. A second run using the discharge of 19,000 cfs and an n value of 0.014 was made using a different Petrov-Galerkin weighting parameter for smooth flow, β_{SM}. This simulation used a β_{SM} of 0.25 rather than a β_{SM} of 0.1, which was used in the initial simulation. The β_{SM} is the minimum damping parameter used throughout the flow field.

The results obtained from the two β_{SM}'s are compared in Plate 6. These profiles show that the variation of β_{SM} resulted in only minor changes in the computed depths. Moreover, the two runs converged to practically the same solution 150 ft downstream of the crest. Therefore, it is apparent that the solution of this particular flow field is not significantly influenced by the choice of the Petrov-Galerkin weighting parameter, β_{SM}.

The model's simulation of the flow in the crest vicinity was further analyzed by grid refinement. The density of the original mesh was doubled in both directions on and adjacent to the crest. Details of the original and

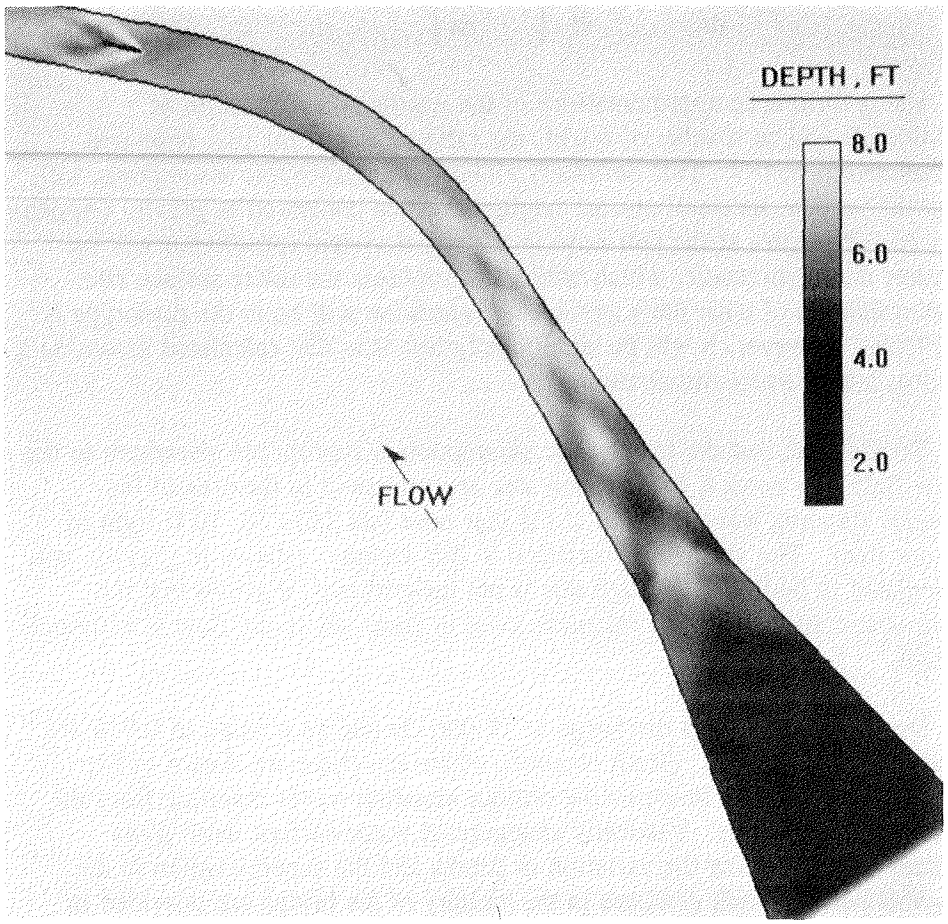

Figure 2. Depth contours for the design discharge (n = 0.014)

refined grids in this area are provided in Plate 7.

Water-surface profiles for the design discharge and an n value of 0.014 computed using the refined grid are shown in Plate 8 and Table 2. The refined solution also oscillated at the crest. The results obtained from the original and fine grids (β_{SM} = 0.1 for both tests) are compared in Plate 9. Again it is apparent that a node-to-node oscillation occurred upstream and downstream of the point at which the flow was accelerating from subcritical to supercritical regardless of grid refinement. The oscillations were pronounced only at the sidewalls where the flow passed around the wing walls and intercepted the converging sidewalls. Therefore, it is difficult to determine whether these results are a numerical artifact or physical. However, the solutions converged at a distance of 150 ft downstream of the crest. Therefore, using the original grid and a β_{SM} of 0.1 are adequate for design purposes and were used throughout the remainder of the study.

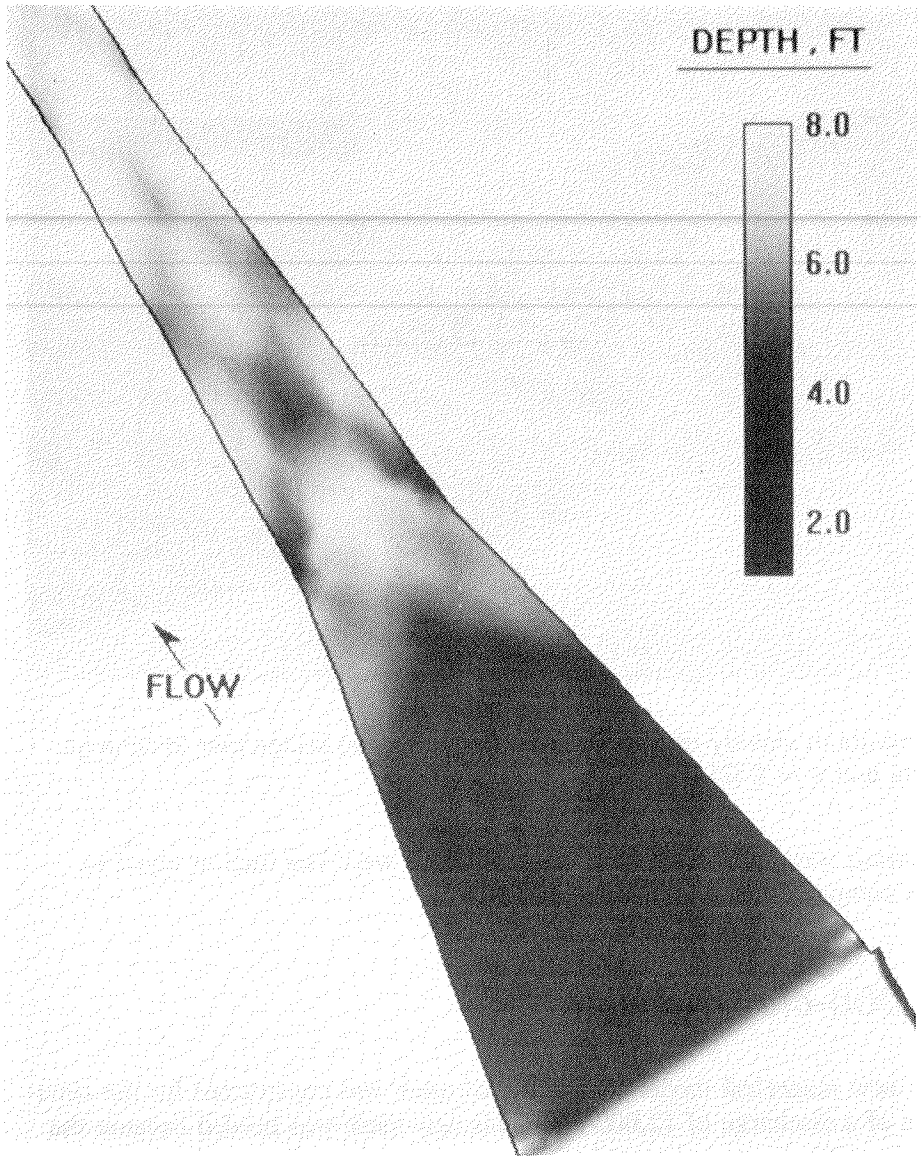

Figure 3. Depth contours within the chute (discharge = 19,000 cfs and n = 0.014)

Decreased roughness (n = 0.012)

Water-surface profiles produced by a discharge of 19,000 cfs and an n value of 0.012 are presented in Plate 10 and Table 3. The reduced n value resulted in the heights of the standing waves being about the same, but the wave crests were located further downstream compared to those from an n value of 0.014. The flow conditions within the reach are much more dependent on the channel form rather than channel friction; that is, the converging sidewalls in the chute, the horizontal curve, and the bridge pier had such an effect on the flow that the differences in an n value of 0.012 compared to an n value of 0.014 were insignificant. The maximum water-surface

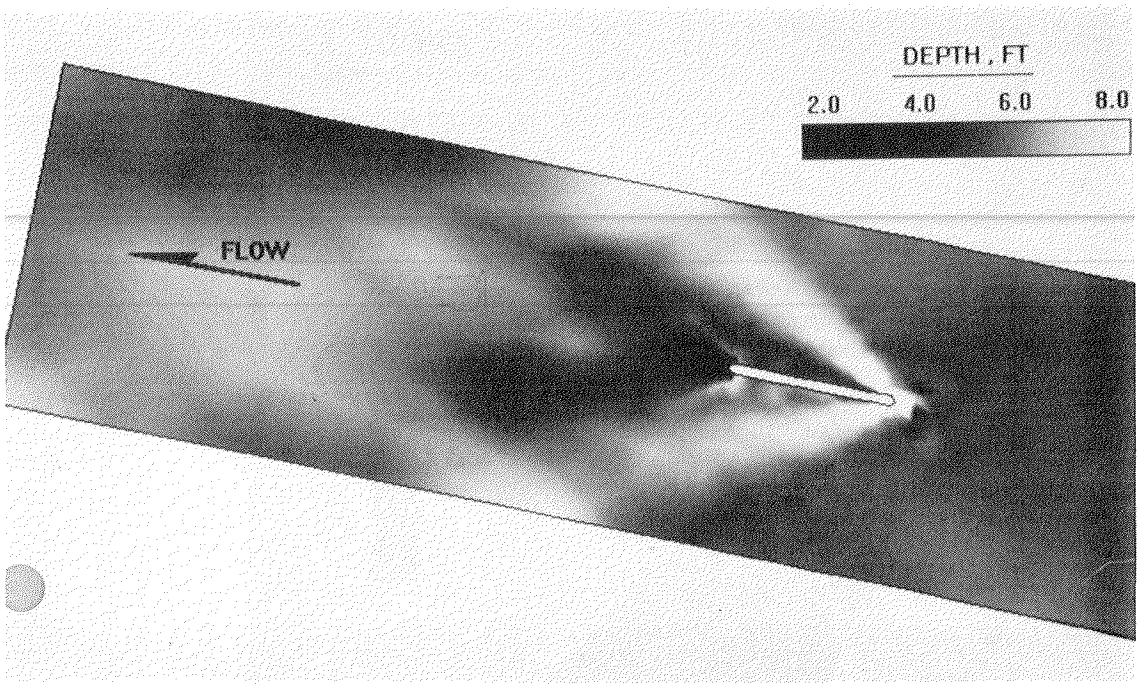

Figure 4. Depth contours in vicinity of San Timoteo Canyon Road bridge pier (discharge 19,000 cfs and n = 0.014)

elevations computed using an n value of 0.012 were less than or equal to those computed using an n value of 0.014.

12,000-cfs Discharge

A new numerical model computational mesh was constructed for the simulation of a discharge of 12,000 cfs. This new mesh was needed because the domain width in the sediment basin was reduced from that resulting from a discharge of 19,000 cfs. The top bank elevation was selected by first determining the expected water-surface elevation in the basin for a discharge of 12,000 cfs. Given the water-surface elevation simulated for a discharge of 19,000 cfs, a discharge coefficient for the "broad-crested weir" was calculated. This discharge coefficient was then used to compute the basin water-surface elevation for a discharge of 12,000 cfs. It was then determined that a top bank elevation of 1314.0 was appropriate to use to construct the grid for the lesser discharge. The numerical model computational mesh for a discharge of 12,000 cfs differed from the original mesh only in the vicinity of the side boundaries within the basin.

Simulation results with a discharge of 12,000 cfs for n values of 0.014 and 0.012 are presented as water-surface profiles in Plates 11 and 12 and Tables 4 and 5, respectively. As expected, the depths are less than those produced by the design discharge and no adverse standing waves were noted. The

maximum water-surface elevations resulting from a discharge of 12,000 cfs using either an n value of 0.014 or an n value of 0.012 were less than those computed for the design discharge with an n value of 0.014.

5 Summary and Conclusions

Two-dimensional (depth-averaged) simulations of the flow conditions in the San Timoteo Channel were conducted to assess the adequacy of the proposed design. Particular attention was given to the variation in flow depths within the entrance chute. The flow at the crest accelerated from subcritical to supercritical flow and remained supercritical through the chute and channel thereafter. Oblique standing waves were produced when the supercritical flow intercepted the chute's laterally converging sidewalls. However, these standing waves were expected and given that the sidewalls will be designed of sufficient height, the flow conditions were deemed acceptable.

The prototype flow geometry and boundary roughness will most likely result in a Manning's n value approximately equal to 0.014. However, flow conditions resulting from a Manning's n value of 0.012 were also simulated so that an envelope of possible hydraulic conditions could be established. Along this same line of reasoning, in addition to the design discharge (19,000 cfs), a smaller discharge (12,000 cfs) was simulated. For a given discharge, there was no significant difference in the water-surface elevations computed using an n value of 0.014 and an n value of 0.012. The smaller n value did, however, result in the wave crests being located further downstream due to the increase in velocity. No adverse flow conditions were noted for a discharge of 12,000 cfs.

Simulation results indicate that the proposed San Timoteo Channel design and in particular, the San Timoteo Canyon Road bridge, will convey the design discharge of 19,000 cfs in an acceptable manner. The prototype will experience significantly less runup on the pier nose than the simulation results indicated. Sidewall heights should be designed based on the simulation results realizing the uncertainties associated with the analyses.

References

Abbott, M. B. (1979). *Computational hydraulics, elements of the theory of free surface flows*. Pitman Advanced Publishing Limited, London.

Berger, R. C. (1993). "A finite element scheme for shock capturing," Technical Report HL-93-12, U.S. Army Engineer Waterways Experiment Station, Vicksburg, MS.

Berger, R. C., and Stockstill, R. L. (1994). "Considerations in 2-D modeling of hydraulically steep flow." *Hydraulic engineering*, Proceedings, 1994 National Conference, ASCE, Buffalo, New York, 1-5 August 1994. New York, 1285-1289.

Rodi, W. (1980). "Turbulence models and their application in hydraulics - A state of the art review," State-of-the Art Paper, International Association for Hydraulic Research, Delft, The Netherlands.

Stockstill, R. L., and Berger, R. C. (1994). "HIVEL2D: A two-dimensional flow model for high-velocity channels," Technical Report REMR-HY-12, U.S. Army Engineer Waterways Experiment Station, Vicksburg, MS.

U.S. Army Engineer District, Los Angeles. (1993). "Santa Ana River Mainstem Project including Santiago Creek; Basis for design - San Timoteo Creek, channel and sediment control structure," Design Memorandum No. 7, Vols 1 and 2, Los Angeles, CA.

Table 1
Water-Surface Elevations, Discharge 19,000 cfs, n = 0.014

Station	Elevation Left Side	Station	Elevation Center	Station	Elevation Right Side
5 + 00.00	1317.45	5 + 00.00	1317.51	5 + 00.00	1317.74
4 + 42.82	1317.56	4 + 40.00	1317.52	4 + 50.89	1317.16
3 + 83.61	1317.54	3 + 80.00	1317.63	3 + 91.28	1317.61
3 + 83.60	1317.51	3 + 20.00	1317.70	3 + 46.00	1317.67
3 + 43.97	1317.68	2 + 72.00	1317.75	2 + 87.60	1317.74
3 + 06.91	1317.80	2 + 24.00	1317.79	2 + 47.99	1317.75
2 + 70.02	1317.82	1 + 88.00	1317.81	2 + 11.60	1317.79
2 + 29.47	1317.88	1 + 64.00	1317.82	1 + 75.99	1317.78
1 + 87.11	1317.78	1 + 40.00	1317.84	1 + 55.55	1317.81
1 + 61.01	1317.77	1 + 16.00	1317.83	1 + 27.99	1317.79
1 + 39.81	1317.85	0 + 92.00	1317.89	1 + 03.99	1317.82
1 + 18.76	1317.83	0 + 68.00	1317.83	0 + 79.99	1317.77
0 + 97.88	1317.85	0 + 44.00	1317.97	0 + 55.39	1317.82
0 + 81.31	1317.84	299 + 16.94	1317.35	0 + 42.45	1317.55
0 + 68.04	1317.80	298 + 96.94	1314.69	0 + 31.32	1317.92
0 + 55.40	1317.87	298 + 76.94	1313.98	299 + 16.94	1317.85
0 + 43.51	1317.64	298 + 46.94	1313.38	299 + 16.94	1317.79
0 + 31.61	1318.02	298 + 22.94	1313.03	299 + 06.94	1314.79
299 + 16.94	1317.92	297 + 90.94	1311.63	298 + 96.94	1317.44
299 + 16.94	1317.77	297 + 58.94	1311.98	298 + 86.94	1315.51
299 + 06.94	1315.51	297 + 26.94	1312.77	298 + 76.94	1315.91
298 + 96.94	1317.38	296 + 96.94	1312.14	298 + 61.94	1315.07
298 + 86.94	1315.93	296 + 66.94	1311.65	298 + 46.94	1314.76
298 + 76.94	1316.00	296 + 36.94	1311.13	298 + 22.94	1314.16
298 + 61.94	1315.32	296 + 06.94	1310.53	297 + 90.94	1313.57
298 + 46.94	1314.95	295 + 74.94	1309.90	297 + 58.94	1312.91
298 + 22.94	1314.34	295 + 45.61	1309.75	297 + 26.94	1312.39
297 + 90.94	1313.68	295 + 16.28	1308.97	296 + 96.94	1311.60
297 + 58.94	1313.03	294 + 86.94	1308.28	296 + 66.94	1311.27
297 + 26.94	1312.47	294 + 46.94	1308.29	296 + 36.94	1310.47
296 + 96.94	1311.75	294 + 06.94	1308.24	296 + 06.94	1309.45
296 + 66.94	1311.31	293 + 64.94	1307.38	295 + 74.94	1310.02
296 + 36.94	1310.51	293 + 22.94	1305.26	295 + 45.61	1310.23
296 + 06.94	1309.70	292 + 80.94	1302.82	295 + 16.28	1310.01
295 + 74.94	1309.99	292 + 38.94	1301.92	294 + 86.94	1309.64
295 + 45.61	1310.13	291 + 96.94	1302.10	294 + 46.94	1308.50
295 + 16.28	1309.92	291 + 54.94	1301.81	294 + 26.94	1308.13
294 + 86.94	1309.52	291 + 12.94	1299.90	294 + 06.94	1306.86
294 + 46.94	1308.40	290 + 70.94	1297.82	293 + 85.94	1304.79
294 + 26.94	1308.08	290 + 28.94	1297.11	293 + 64.94	1305.07
294 + 06.94	1306.76	290 + 07.94	1297.11	293 + 22.94	1305.32
293 + 85.94	1304.68	289 + 86.94	1297.11	292 + 80.94	1304.65
293 + 64.94	1305.01	289 + 66.29	1296.89	292 + 38.94	1303.35
293 + 22.94	1305.38	289 + 45.64	1296.49	291 + 96.94	1301.28

(Continued)

Note: Sides of channel are referenced to looking downstream.

Table 1 (Concluded)

Station	Elevation Left Side	Station	Elevation Center	Station	Elevation Right Side
292 + 38.94	1303.42	288 + 70.26	1293.77	291 + 12.94	1299.80
291 + 96.94	1301.38	288 + 36.92	1293.27	290 + 70.94	1299.18
291 + 54.94	1299.80	288 + 03.59	1293.76	290 + 28.94	1297.77
291 + 12.94	1299.66	287 + 61.97	1293.71	290 + 07.94	1297.35
290 + 70.94	1299.11	287 + 20.35	1292.78	289 + 86.94	1296.37
290 + 28.94	1297.78	286 + 78.74	1291.78	289 + 66.29	1294.72
290 + 07.94	1297.39	286 + 37.12	1291.29	289 + 45.64	1294.44
289 + 86.94	1296.20	285 + 95.50	1291.04	289 + 03.59	1295.31
289 + 66.29	1294.78	285 + 53.88	1290.68	288 + 70.26	1296.03
289 + 45.64	1294.46	285 + 12.26	1290.07	288 + 36.92	1295.63
289 + 03.59	1295.34	284 + 70.64	1289.44	288 + 03.59	1295.48
288 + 70.26	1294.11	284 + 29.03	1288.87	287 + 61.97	1294.68
288 + 36.92	1292.63	283 + 87.41	1288.43	287 + 20.35	1294.26
288 + 03.59	1291.11	283 + 45.79	1287.89	286 + 78.74	1293.96
287 + 61.97	1290.65	283 + 12.46	1287.49	286 + 37.12	1293.57
287 + 20.35	1290.68	282 + 79.12	1286.99	285 + 95.50	1293.17
286 + 78.74	1290.26	282 + 62.46	1286.65	285 + 53.88	1292.68
286 + 37.12	1289.32	282 + 45.79	1286.44	285 + 12.26	1292.32
285 + 95.50	1288.37	282 + 38.08	1286.43	284 + 70.64	1291.80
285 + 53.88	1287.70	282 + 30.38	1286.15	284 + 29.03	1291.04
285 + 12.26	1287.28	282 + 25.25	1285.51	283 + 87.41	1290.37
284 + 70.64	1286.94	282 + 20.12	1295.03	283 + 45.79	1289.82
284 + 29.03	1286.56	281 + 76.12	1282.46	283 + 12.46	1288.67
283 + 87.41	1286.14	281 + 75.50	1281.66	282 + 79.12	1287.03
283 + 45.79	1285.63	281 + 71.89	1283.52	282 + 62.46	1287.00
283 + 12.46	1286.01	281 + 65.46	1284.70	282 + 45.79	1286.79
282 + 79.12	1286.52	281 + 59.22	1285.35	282 + 32.98	1286.64
282 + 62.46	1286.77	281 + 50.18	1285.78	282 + 20.12	1286.52
282 + 45.79	1286.81	281 + 39.32	1286.22	282 + 09.11	1286.37
282 + 32.98	1286.39	281 + 23.85	1285.84	281 + 98.11	1286.62
282 + 20.12	1286.22	280 + 95.40	1285.89	281 + 87.10	1286.17
282 + 09.11	1286.12	280 + 63.60	1286.07	281 + 76.09	1286.30
281 + 98.11	1285.97	280 + 31.80	1285.75	281 + 59.61	1287.43
281 + 87.10	1286.01	280 + 00.00	1285.20	281 + 43.10	1287.38
281 + 76.09	1285.38			281 + 27.20	1286.27
281 + 59.61	1285.86			280 + 95.40	1285.06
281 + 43.10	1287.03			280 + 63.60	1284.93
281 + 27.20	1286.71			280 + 31.80	1285.13
280 + 95.40	1285.25			280 + 00.00	1285.36
280 + 63.60	1285.03				
280 + 31.80	1285.38				
280 + 00.00	1285.92				

Table 2
Water-Surface Elevations, Discharge 19,000 cfs, n = 0.014, Fine Grid

Station	Elevation Left Side	Station	Elevation Center	Station	Elevation Right Side
5 + 00.00	1317.34	5 + 00.00	1317.40	5 + 00.00	1317.66
4 + 42.82	1317.45	4 + 40.00	1317.42	4 + 50.89	1317.03
3 + 83.61	1317.43	3 + 80.00	1317.52	3 + 91.28	1317.50
3 + 83.60	1317.39	3 + 20.00	1317.59	3 + 46.00	1317.57
3 + 43.97	1317.57	2 + 72.00	1317.65	2 + 87.60	1317.62
3 + 06.91	1317.69	2 + 24.00	1317.69	2 + 47.99	1317.65
2 + 70.02	1317.71	1 + 88.00	1317.70	2 + 11.60	1317.67
2 + 29.47	1317.78	1 + 64.00	1317.72	1 + 75.99	1317.69
1 + 87.11	1317.67	1 + 40.00	1317.73	1 + 55.55	1317.70
1 + 61.01	1317.67	1 + 16.00	1317.74	1 + 27.99	1317.70
1 + 39.81	1317.74	0 + 92.00	1317.76	1 + 03.99	1317.71
1 + 18.76	1317.74	0 + 68.00	1317.77	0 + 79.99	1317.68
0 + 97.88	1317.73	0 + 44.00	1317.78	0 + 55.39	1317.70
0 + 81.31	1317.74	0 + 32.00	1317.71	0 + 42.45	1317.47
0 + 68.04	1317.69	299 + 16.94	1316.98	0 + 31.32	1317.80
0 + 55.40	1317.76	299 + 06.94	1314.92	299 + 16.94	1317.68
0 + 43.51	1317.55	298 + 96.94	1314.87	299 + 16.94	1317.77
0 + 31.61	1317.91	298 + 76.94	1314.11	299 + 11.94	1314.02
299 + 16.94	1317.65	298 + 46.94	1313.47	299 + 06.94	1317.14
299 + 16.94	1317.88	298 + 22.94	1312.83	299 + 01.94	1315.68
299 + 11.94	1315.11	297 + 90.94	1311.91	298 + 96.94	1316.77
299 + 06.94	1317.18	297 + 58.94	1312.44	298 + 91.94	1316.08
299 + 01.94	1316.10	297 + 26.94	1312.67	298 + 86.94	1316.00
298 + 96.94	1316.91	296 + 96.94	1312.09	298 + 81.94	1315.72
298 + 91.94	1316.36	296 + 66.94	1311.64	298 + 76.94	1315.55
298 + 86.94	1316.19	296 + 36.94	1311.05	298 + 66.94	1315.30
298 + 81.94	1315.96	296 + 06.94	1310.52	298 + 46.94	1314.73
298 + 76.94	1315.78	295 + 74.94	1309.96	298 + 22.94	1314.21
298 + 66.94	1315.51	295 + 45.61	1309.74	297 + 90.94	1313.55
298 + 46.94	1314.93	295 + 16.28	1308.87	297 + 58.94	1312.94
298 + 22.94	1314.38	294 + 86.94	1308.44	297 + 26.94	1312.35
297 + 90.94	1313.69	294 + 46.94	1308.54	296 + 96.94	1311.68
297 + 58.94	1313.05	294 + 06.94	1308.15	296 + 66.94	1311.23
297 + 26.94	1312.47	293 + 64.94	1307.28	296 + 36.94	1310.29
296 + 96.94	1311.81	293 + 22.94	1305.23	296 + 06.94	1309.67
296 + 66.94	1311.27	292 + 80.94	1302.88	295 + 74.94	1310.33
296 + 36.94	1310.43	292 + 38.94	1302.03	295 + 45.61	1310.19
296 + 06.94	1309.89	291 + 96.94	1302.10	295 + 16.28	1310.00
295 + 74.94	1310.23	291 + 54.94	1301.71	294 + 86.94	1309.63
295 + 45.61	1310.11	291 + 12.94	1299.83	294 + 46.94	1308.39
295 + 16.28	1309.88	290 + 70.94	1297.87	294 + 26.94	1308.08
294 + 86.94	1309.50	290 + 28.94	1297.20	294 + 06.94	1306.88
294 + 46.94	1308.30	290 + 07.94	1297.13	293 + 85.94	1304.85

(Continued)

Note: Sides of channel are referenced to looking downstream.

Table 2 (Concluded)					
Station	Elevation Left Side	Station	Elevation Center	Station	Elevation Right Side
294 + 26.94	1308.01	289 + 86.94	1297.09	293 + 64.94	1305.26
294 + 06.94	1306.76	289 + 66.29	1296.88	293 + 22.94	1305.32
293 + 85.94	1304.71	289 + 45.64	1296.38	292 + 80.94	1304.58
293 + 64.94	1305.23	289 + 03.59	1294.99	292 + 38.94	1303.28
293 + 22.94	1305.40	288 + 70.26	1293.92	291 + 96.94	1301.27
292 + 80.94	1304.67	288 + 36.92	1293.39	291 + 54.94	1299.90
292 + 38.94	1303.36	288 + 03.59	1293.74	291 + 12.94	1299.83
291 + 96.94	1301.38	287 + 61.97	1293.67	290 + 70.94	1299.13
291 + 54.94	1299.88	287 + 20.35	1292.76	290 + 28.94	1297.73
291 + 12.94	1299.67	286 + 78.74	1291.81	290 + 07.94	1297.52
290 + 70.94	1299.05	286 + 37.12	1291.32	289 + 86.94	1296.11
290 + 28.94	1297.80	285 + 95.50	1291.06	289 + 66.29	1294.81
290 + 07.94	1297.24	285 + 53.88	1290.67	289 + 45.64	1294.55
289 + 86.94	1296.15	285 + 12.26	1290.06	289 + 03.59	1295.26
289 + 66.29	1294.92	284 + 70.64	1289.44	288 + 70.26	1296.03
289 + 45.64	1294.74	284 + 29.03	1288.89	288 + 36.92	1295.63
289 + 03.59	1295.14	283 + 87.41	1288.43	288 + 03.59	1295.48
288 + 70.26	1294.07	283 + 45.79	1287.89	287 + 61.97	1294.72
288 + 36.92	1292.74	283 + 12.46	1287.49	287 + 20.35	1294.29
288 + 03.59	1291.14	282 + 79.12	1286.98	286 + 78.74	1293.94
287 + 61.97	1290.64	282 + 62.46	1286.64	286 + 37.12	1293.58
287 + 20.35	1290.67	282 + 45.79	1286.47	285 + 95.50	1293.14
286 + 78.74	1290.25	282 + 38.08	1286.44	285 + 53.88	1292.74
286 + 37.12	1289.32	282 + 30.38	1286.17	285 + 12.26	1292.31
285 + 95.50	1288.38	282 + 25.25	1285.47	284 + 70.64	1291.74
285 + 53.88	1287.73	282 + 20.12	1295.00	284 + 29.03	1291.05
285 + 12.26	1287.30	281 + 76.12	1282.46	283 + 87.41	1290.38
284 + 70.64	1286.94	281 + 75.50	1281.62	283 + 45.79	1289.83
284 + 29.03	1286.55	281 + 71.89	1283.48	283 + 12.46	1288.70
283 + 87.41	1286.14	281 + 65.46	1284.66	282 + 79.12	1287.05
283 + 45.79	1285.63	281 + 59.22	1285.33	282 + 62.46	1286.95
283 + 12.46	1286.01	281 + 50.18	1285.84	282 + 45.79	1286.76
282 + 79.12	1286.51	281 + 39.32	1286.07	282 + 32.98	1286.67
282 + 62.46	1286.72	281 + 23.85	1285.85	282 + 20.12	1286.53
282 + 45.79	1286.84	280 + 95.40	1285.85	282 + 09.11	1286.37
282 + 32.98	1286.43	280 + 63.60	1286.11	281 + 98.11	1286.59
282 + 20.12	1286.23	280 + 31.80	1285.78	281 + 87.10	1286.18
282 + 09.11	1286.13	280 + 00.00	1285.18	281 + 76.09	1286.33
281 + 98.11	1285.95			281 + 59.61	1287.48
281 + 87.10	1286.03			281 + 43.10	1287.34
281 + 76.09	1285.35			281 + 27.20	1286.35
281 + 59.61	1285.92			280 + 95.40	1284.96
281 + 43.10	1286.97			280 + 63.60	1284.9
281 + 27.20	1286.75			280 + 31.80	1285.31
280 + 95.40	1285.23			280 + 00.00	1285.32
280 + 63.60	1285.10				
280 + 31.80	1285.90				
280 + 00.00	1285.36				

Table 3
Water-Surface Elevations, Discharge 19,000 cfs, n = 0.012

Station	Elevation Left Side	Station	Elevation Center	Station	Elevation Right Side
5 + 00.00	1317.44	5 + 00.00	1317.50	5 + 00.00	1317.74
4 + 42.82	1317.55	4 + 40.00	1317.52	4 + 50.89	1317.15
3 + 83.61	1317.54	3 + 80.00	1317.62	3 + 91.28	1317.60
3 + 83.60	1317.50	3 + 20.00	1317.69	3 + 46.00	1317.66
3 + 43.97	1317.67	2 + 72.00	1317.75	2 + 87.60	1317.73
3 + 06.91	1317.79	2 + 24.00	1317.78	2 + 47.99	1317.74
2 + 70.02	1317.81	1 + 88.00	1317.80	2 + 11.60	1317.78
2 + 29.47	1317.87	1 + 64.00	1317.81	1 + 75.99	1317.77
1 + 87.11	1317.77	1 + 40.00	1317.83	1 + 55.55	1317.80
1 + 61.01	1317.76	1 + 16.00	1317.83	1 + 27.99	1317.78
1 + 39.81	1317.84	0 + 92.00	1317.88	1 + 03.99	1317.82
1 + 18.76	1317.82	0 + 68.00	1317.82	0 + 79.99	1317.76
0 + 97.88	1317.84	0 + 44.00	1317.96	0 + 55.39	1317.82
0 + 81.31	1317.83	299 + 16.94	1317.34	0 + 42.45	1317.54
0 + 68.04	1317.79	298 + 96.94	1314.68	0 + 31.32	1317.92
0 + 55.40	1317.86	298 + 76.94	1313.97	299 + 16.94	1317.85
0 + 43.51	1317.63	298 + 46.94	1313.30	299 + 16.94	1317.77
0 + 31.61	1318.02	298 + 22.94	1313.01	299 + 06.94	1314.74
299 + 16.94	1317.77	297 + 90.94	1311.71	298 + 96.94	1317.46
299 + 16.94	1317.91	297 + 58.94	1311.52	298 + 86.94	1315.45
299 + 06.94	1315.48	297 + 26.94	1312.64	298 + 76.94	1315.91
298 + 96.94	1317.39	296 + 96.94	1312.12	298 + 61.94	1315.03
298 + 86.94	1315.89	296 + 66.94	1311.50	298 + 46.94	1314.75
298 + 76.94	1316.00	296 + 36.94	1311.11	298 + 22.94	1314.11
298 + 61.94	1315.29	296 + 06.94	1310.55	297 + 90.94	1313.53
298 + 46.94	1314.94	295 + 74.94	1309.81	297 + 58.94	1312.84
298 + 22.94	1314.29	295 + 45.61	1309.43	297 + 26.94	1312.35
297 + 90.94	1313.64	295 + 16.28	1309.02	296 + 96.94	1311.55
297 + 58.94	1312.98	294 + 86.94	1308.26	296 + 66.94	1311.04
297 + 26.94	1312.42	294 + 46.94	1307.40	296 + 36.94	1310.62
296 + 96.94	1311.69	294 + 06.94	1307.87	296 + 06.94	1309.40
296 + 66.94	1311.15	293 + 64.94	1307.68	295 + 74.94	1309.26
296 + 36.94	1310.61	293 + 22.94	1305.41	295 + 45.61	1309.97
296 + 06.94	1309.61	292 + 80.94	1302.89	295 + 16.28	1309.86
295 + 74.94	1309.38	292 + 38.94	1301.21	294 + 86.94	1309.46
295 + 45.61	1309.85	291 + 96.94	1301.12	294 + 46.94	1308.53
295 + 16.28	1309.78	291 + 54.94	1301.79	294 + 26.94	1308.23
294 + 86.94	1309.37	291 + 12.94	1300.68	294 + 06.94	1306.84
294 + 46.94	1308.39	290 + 70.94	1298.05	293 + 85.94	1304.79
294 + 26.94	1308.13	290 + 28.94	1296.36	293 + 64.94	1304.28
294 + 06.94	1306.73	290 + 07.94	1295.99	293 + 22.94	1304.77
293 + 85.94	1304.73	289 + 86.94	1296.19	292 + 80.94	1304.49
293 + 64.94	1304.18	289 + 66.29	1296.26	292 + 38.94	1303.63
293 + 22.94	1304.70	289 + 45.64	1296.82	291 + 96.94	1301.63

(Continued)

Note: Sides of channel are referenced to looking downstream.

Table 3 (Concluded)					
Station	Elevation Left Side	Station	Elevation Center	Station	Elevation Right Side
292 + 80.94	1304.62	289 + 03.59	1295.65	291 + 54.94	1299.34
292 + 38.94	1303.72	288 + 70.26	1293.85	291 + 12.94	1298.91
291 + 96.94	1301.68	288 + 36.92	1292.55	290 + 70.94	1299.06
291 + 54.94	1299.45	288 + 03.59	1292.74	290 + 28.94	1298.00
291 + 12.94	1298.81	287 + 61.97	1293.40	290 + 07.94	1297.35
290 + 70.94	1298.93	287 + 20.35	1292.98	289 + 86.94	1296.28
290 + 28.94	1298.00	286 + 78.74	1291.83	289 + 66.29	1294.50
290 + 07.94	1297.39	286 + 37.12	1290.83	289 + 45.64	1293.76
289 + 86.94	1296.35	285 + 95.50	1290.44	289 + 03.59	1295.04
289 + 66.29	1294.28	285 + 53.88	1290.33	288 + 70.26	1295.79
289 + 45.64	1293.95	285 + 12.26	1289.96	288 + 36.92	1295.60
289 + 03.59	1294.81	284 + 70.64	1289.28	288 + 03.59	1295.55
288 + 70.26	1293.77	284 + 29.03	1288.52	287 + 61.97	1294.57
288 + 36.92	1292.81	283 + 87.41	1287.97	287 + 20.35	1293.96
288 + 03.59	1291.05	283 + 45.79	1287.51	286 + 78.74	1293.86
287 + 61.97	1290.06	283 + 12.46	1287.20	286 + 37.12	1293.70
287 + 20.35	1289.79	282 + 79.12	1286.73	285 + 95.50	1293.18
286 + 78.74	1289.65	282 + 62.46	1286.39	285 + 53.88	1292.57
286 + 37.12	1289.01	282 + 45.79	1286.17	285 + 12.26	1292.06
285 + 95.50	1288.02	282 + 38.08	1286.12	284 + 70.64	1291.60
285 + 53.88	1287.13	282 + 30.38	1285.85	284 + 29.03	1291.08
285 + 12.26	1286.59	282 + 25.25	1285.15	283 + 87.41	1290.44
284 + 70.64	1286.33	282 + 20.12	1294.72	283 + 45.79	1289.81
284 + 29.03	1286.02	281 + 76.12	1282.46	283 + 12.46	1288.59
283 + 87.41	1285.55	281 + 75.50	1281.35	282 + 79.12	1286.83
283 + 45.79	1284.94	281 + 71.89	1282.94	282 + 62.46	1286.67
283 + 12.46	1285.31	281 + 65.46	1284.10	282 + 45.79	1286.46
282 + 79.12	1285.88	281 + 59.22	1284.84	282 + 32.98	1286.34
282 + 62.46	1286.17	281 + 50.18	1285.30	282 + 20.12	1286.19
282 + 45.79	1286.46	281 + 39.32	1285.78	282 + 09.11	1286.02
282 + 32.98	1286.06	281 + 23.85	1285.72	281 + 98.11	1286.08
282 + 20.12	1285.83	280 + 95.40	1285.43	281 + 87.10	1286.10
282 + 09.11	1285.84	280 + 63.60	1285.57	281 + 76.09	1285.47
281 + 98.11	1285.72	280 + 31.80	1285.51	281 + 59.61	1286.47
281 + 87.10	1285.84	280 + 00.00	1285.03	281 + 43.10	1287.08
281 + 76.09	1285.37			281 + 27.20	1286.41
281 + 59.61	1285.37			280 + 95.40	1284.80
281 + 43.10	1286.37			280 + 63.60	1284.37
281 + 27.20	1286.53			280 + 31.80	1284.59
280 + 95.40	1284.99			280 + 00.00	1284.71
280 + 63.60	1284.49				
280 + 31.80	1284.62				
280 + 00.00	1284.86				

Table 4
Water-Surface Elevations, Discharge 12,000 cfs, n = 0.014

Station	Elevation Left Side	Station	Elevation Center	Station	Elevation Right Side
5 + 00.00	1315.82	5 + 00.00	1315.89	5 + 00.00	1315.99
4 + 42.82	1315.94	4 + 40.00	1315.90	4 + 50.89	1315.72
3 + 83.61	1315.93	3 + 80.00	1315.95	3 + 91.28	1315.95
3 + 83.60	1315.91	3 + 20.00	1315.99	3 + 46.00	1315.97
3 + 43.97	1315.96	2 + 72.00	1316.02	2 + 87.60	1316.01
3 + 06.91	1316.05	2 + 24.00	1316.04	2 + 47.99	1316.01
2 + 70.02	1316.05	1 + 88.00	1316.05	2 + 11.60	1316.04
2 + 29.47	1316.08	1 + 64.00	1316.05	1 + 75.99	1316.03
1 + 87.11	1316.04	1 + 40.00	1316.06	1 + 55.55	1316.05
1 + 61.01	1316.03	1 + 16.00	1316.06	1 + 27.99	1316.03
1 + 39.81	1316.07	0 + 92.00	1316.09	1 + 03.99	1316.06
1 + 18.76	1316.05	0 + 68.00	1316.05	0 + 79.99	1316.02
0 + 97.88	1316.07	0 + 44.00	1316.15	0 + 55.39	1316.03
0 + 81.31	1316.05	299 + 16.94	1315.74	0 + 42.45	1315.94
0 + 68.04	1316.03	298 + 96.94	1313.61	0 + 31.32	1315.98
0 + 55.40	1316.07	298 + 76.94	1313.04	299 + 16.94	1315.72
0 + 43.51	1315.94	298 + 46.94	1312.35	299 + 16.94	1315.78
0 + 31.61	1316.09	298 + 22.94	1312.00	299 + 06.94	1314.50
299 + 16.94	1316.01	297 + 90.94	1311.32	298 + 96.94	1315.44
299 + 16.94	1315.80	297 + 58.94	1310.41	298 + 86.94	1314.50
299 + 06.94	1314.54	297 + 26.94	1310.81	298 + 76.94	1314.25
298 + 96.94	1315.54	296 + 96.94	1310.91	298 + 61.94	1313.81
298 + 86.94	1314.58	296 + 66.94	1310.21	298 + 46.94	1313.45
298 + 76.94	1314.40	296 + 36.94	1309.69	298 + 22.94	1312.95
298 + 61.94	1313.91	296 + 06.94	1309.32	297 + 90.94	1312.31
298 + 46.94	1313.57	295 + 74.94	1308.76	297 + 58.94	1311.81
298 + 22.94	1313.03	295 + 45.61	1308.22	297 + 26.94	1311.19
297 + 90.94	1312.40	295 + 16.28	1307.87	296 + 96.94	1310.71
297 + 58.94	1311.85	294 + 86.94	1307.34	296 + 66.94	1309.90
297 + 26.94	1311.27	294 + 46.94	1306.11	296 + 36.94	1309.60
296 + 96.94	1310.72	294 + 06.94	1305.15	296 + 06.94	1308.89
296 + 66.94	1310.01	293 + 64.94	1305.51	295 + 74.94	1308.05
296 + 36.94	1309.61	293 + 22.94	1303.99	295 + 45.61	1307.92
296 + 06.94	1308.91	292 + 80.94	1301.95	295 + 16.28	1308.12
295 + 74.94	1308.16	292 + 38.94	1300.15	294 + 86.94	1307.87
295 + 45.61	1308.01	291 + 96.94	1298.64	294 + 46.94	1306.76
295 + 16.28	1308.06	291 + 54.94	1298.45	294 + 26.94	1306.58
294 + 86.94	1307.83	291 + 12.94	1298.29	294 + 06.94	1305.65
294 + 46.94	1306.74	290 + 70.94	1297.19	293 + 85.94	1303.88
294 + 26.94	1306.52	290 + 28.94	1295.70	293 + 64.94	1303.43
294 + 06.94	1305.58	290 + 07.94	1294.70	293 + 22.94	1302.57
293 + 85.94	1303.78	289 + 86.94	1293.91	292 + 80.94	1302.00
293 + 64.94	1303.47	289 + 66.29	1293.44	292 + 38.94	1301.65
293 + 22.94	1302.49	289 + 45.64	1293.36	291 + 96.94	1300.41

(Continued)

Note: Sides of channel are referenced to looking downstream.

Table 4 (Concluded)

Station	Elevation Left Side	Station	Elevation Center	Station	Elevation Right Side
292 + 80.94	1301.88	289 + 03.59	1293.15	291 + 54.94	1298.48
292 + 38.94	1301.73	288 + 70.26	1292.56	291 + 12.94	1297.06
291 + 96.94	1300.45	288 + 36.92	1291.70	290 + 70.94	1296.21
291 + 54.94	1298.46	288 + 03.59	1291.28	290 + 28.94	1295.72
291 + 12.94	1297.18	287 + 61.97	1291.14	290 + 07.94	1295.72
290 + 70.94	1296.24	287 + 20.35	1290.76	289 + 86.94	1294.41
290 + 28.94	1295.63	286 + 78.74	1290.12	289 + 66.29	1293.29
290 + 07.94	1295.70	286 + 37.12	1289.48	289 + 45.64	1292.65
289 + 86.94	1294.42	285 + 95.50	1288.95	289 + 03.59	1292.43
289 + 66.29	1293.30	285 + 53.88	1288.52	288 + 70.26	1293.67
289 + 45.64	1292.70	285 + 12.26	1288.09	288 + 36.92	1293.63
289 + 03.59	1292.47	284 + 70.64	1287.63	288 + 03.59	1293.39
288 + 70.26	1291.57	284 + 29.03	1287.11	287 + 61.97	1292.70
288 + 36.92	1290.75	283 + 87.41	1286.59	287 + 20.35	1291.94
288 + 03.59	1289.58	283 + 45.79	1286.02	286 + 78.74	1291.22
287 + 61.97	1288.97	283 + 12.46	1285.64	286 + 37.12	1290.90
287 + 20.35	1288.79	282 + 79.12	1285.18	285 + 95.50	1290.62
286 + 78.74	1288.63	282 + 62.46	1284.86	285 + 53.88	1290.29
286 + 37.12	1288.09	282 + 45.79	1284.72	285 + 12.26	1289.96
285 + 95.50	1287.31	282 + 38.08	1284.68	284 + 70.64	1289.54
285 + 53.88	1286.50	282 + 30.38	1284.48	284 + 29.03	1288.98
285 + 12.26	1285.79	282 + 25.25	1283.94	283 + 87.41	1288.33
284 + 70.64	1285.22	282 + 20.12	1291.17	283 + 45.79	1287.68
284 + 29.03	1284.81	281 + 76.12	1281.01	283 + 12.46	1286.43
283 + 87.41	1284.53	281 + 75.50	1280.98	282 + 79.12	1284.79
283 + 45.79	1284.21	281 + 71.89	1282.37	282 + 62.46	1284.66
283 + 12.46	1284.72	281 + 65.46	1283.48	282 + 45.79	1284.50
282 + 79.12	1285.22	281 + 59.22	1284.00	282 + 32.98	1284.37
282 + 62.46	1285.41	281 + 50.18	1284.04	282 + 20.12	1284.29
282 + 45.79	1285.43	281 + 39.32	1284.36	282 + 09.11	1284.16
282 + 32.98	1285.06	281 + 23.85	1283.99	281 + 98.11	1284.52
282 + 20.12	1284.80	280 + 95.40	1283.92	281 + 87.10	1284.19
282 + 09.11	1284.72	280 + 63.60	1284.11	281 + 76.09	1284.30
281 + 98.11	1284.43	280 + 31.80	1283.91	281 + 59.61	1285.41
281 + 87.10	1284.50	280 + 00.00	1283.47	281 + 43.10	1285.40
281 + 76.09	1283.90			281 + 27.20	1284.24
281 + 59.61	1284.06			280 + 95.40	1283.29
281 + 43.10	1284.64			280 + 63.60	1283.71
281 + 27.20	1284.88			280 + 31.80	1283.91
280 + 95.40	1283.96			280 + 00.00	1283.64
280 + 63.60	1283.16				
280 + 31.80	1283.37				
280 + 00.00	1283.20				

Table 5
Water-Surface Elevations, Discharge 12,000 cfs, n = 0.012

Station	Elevation Left Side	Station	Elevation Center	Station	Elevation Right Side
5 + 00.00	1315.81	5 + 00.00	1315.89	5 + 00.00	1315.99
4 + 42.82	1315.93	4 + 40.00	1315.89	4 + 50.89	1315.71
3 + 83.61	1315.92	3 + 80.00	1315.95	3 + 91.28	1315.94
3 + 83.60	1315.90	3 + 20.00	1315.98	3 + 46.00	1315.96
3 + 43.97	1315.96	2 + 72.00	1316.01	2 + 87.60	1316.00
3 + 06.91	1316.05	2 + 24.00	1316.03	2 + 47.99	1316.01
2 + 70.02	1316.04	1 + 88.00	1316.04	2 + 11.60	1316.03
2 + 29.47	1316.08	1 + 64.00	1316.05	1 + 75.99	1316.02
1 + 87.11	1316.03	1 + 40.00	1316.06	1 + 55.55	1316.05
1 + 61.01	1316.02	1 + 16.00	1316.05	1 + 27.99	1316.02
1 + 39.81	1316.06	0 + 92.00	1316.09	1 + 03.99	1316.05
1 + 18.76	1316.05	0 + 68.00	1316.04	0 + 79.99	1316.01
0 + 97.88	1316.06	0 + 44.00	1316.14	0 + 55.39	1316.02
0 + 81.31	1316.05	299 + 16.94	1315.74	0 + 42.45	1315.93
0 + 68.04	1316.03	298 + 96.94	1313.59	0 + 31.32	1315.97
0 + 55.40	1316.07	298 + 76.94	1313.03	299 + 16.94	1315.71
0 + 43.51	1315.94	298 + 46.94	1312.32	299 + 16.94	1315.77
0 + 31.61	1316.08	298 + 22.94	1311.90	299 + 06.94	1314.49
299 + 16.94	1316.00	297 + 90.94	1311.34	298 + 96.94	1315.45
299 + 16.94	1315.79	297 + 58.94	1310.38	298 + 86.94	1314.48
299 + 06.94	1314.53	297 + 26.94	1310.32	298 + 76.94	1314.24
298 + 96.94	1315.54	296 + 96.94	1310.80	298 + 61.94	1313.78
298 + 86.94	1314.55	296 + 66.94	1310.29	298 + 46.94	1313.41
298 + 76.94	1314.39	296 + 36.94	1309.55	298 + 22.94	1312.92
298 + 61.94	1313.88	296 + 06.94	1309.15	297 + 90.94	1312.26
298 + 46.94	1313.53	295 + 74.94	1308.71	297 + 58.94	1311.76
298 + 22.94	1313.00	295 + 45.61	1308.25	297 + 26.94	1311.13
297 + 90.94	1312.35	295 + 16.28	1307.86	296 + 96.94	1310.64
297 + 58.94	1311.80	294 + 86.94	1307.28	296 + 66.94	1309.90
297 + 26.94	1311.21	294 + 46.94	1306.21	296 + 36.94	1309.41
296 + 96.94	1310.66	294 + 06.94	1304.66	296 + 06.94	1308.88
296 + 66.94	1309.97	293 + 64.94	1304.99	295 + 74.94	1308.16
296 + 36.94	1309.47	293 + 22.94	1304.17	295 + 45.61	1307.38
296 + 06.94	1308.91	292 + 80.94	1302.07	295 + 16.28	1307.55
295 + 74.94	1308.18	292 + 38.94	1300.22	294 + 86.94	1307.81
295 + 45.61	1307.55	291 + 96.94	1298.56	294 + 46.94	1306.68
295 + 16.28	1307.60	291 + 54.94	1297.52	294 + 26.94	1306.31
294 + 86.94	1307.72	291 + 12.94	1297.45	294 + 06.94	1305.55
294 + 46.94	1306.66	290 + 70.94	1297.23	293 + 85.94	1303.75
294 + 26.94	1306.32	290 + 28.94	1295.95	293 + 64.94	1303.60
294 + 06.94	1305.50	290 + 07.94	1295.17	293 + 22.94	1302.51
293 + 85.94	1303.65	289 + 86.94	1294.16	292 + 80.94	1301.26

(Continued)

Note: Sides of channel are referenced to looking downstream.

Table 5 (Concluded)					
Station	Elevation Left Side	Station	Elevation Center	Station	Elevation Right Side
293 + 64.94	1303.52	289 + 66.29	1293.28	292 + 38.94	1301.34
293 + 22.94	1302.51	289 + 45.64	1292.82	291 + 96.94	1300.44
292 + 80.94	1301.12	289 + 03.59	1292.54	291 + 54.94	1298.62
292 + 38.94	1301.30	288 + 70.26	1292.16	291 + 12.94	1297.11
291 + 96.94	1300.46	288 + 36.92	1291.66	290 + 70.94	1295.97
291 + 54.94	1298.66	288 + 03.59	1291.27	290 + 28.94	1295.10
291 + 12.94	1297.17	287 + 61.97	1290.92	290 + 07.94	1294.92
290 + 70.94	1295.99	287 + 20.35	1290.45	289 + 86.94	1294.38
290 + 28.94	1295.10	286 + 78.74	1289.85	289 + 66.29	1293.06
290 + 07.94	1294.94	286 + 37.12	1289.25	289 + 45.64	1292.56
289 + 86.94	1294.44	285 + 95.50	1288.73	289 + 03.59	1292.49
289 + 66.29	1293.10	285 + 53.88	1288.29	288 + 70.26	1293.16
289 + 45.64	1292.63	285 + 12.26	1287.84	288 + 36.92	1293.40
289 + 03.59	1292.45	284 + 70.64	1287.36	288 + 03.59	1293.32
288 + 70.26	1291.31	284 + 29.03	1286.81	287 + 61.97	1292.55
288 + 36.92	1290.36	283 + 87.41	1286.29	287 + 20.35	1292.01
288 + 03.59	1289.13	283 + 45.79	1285.76	286 + 78.74	1291.47
287 + 61.97	1288.48	283 + 12.46	1285.37	286 + 37.12	1290.99
287 + 20.35	1288.15	282 + 79.12	1284.90	285 + 95.50	1290.57
286 + 78.74	1287.91	282 + 62.46	1284.56	285 + 53.88	1290.16
286 + 37.12	1287.45	282 + 45.79	1284.41	285 + 12.26	1289.75
285 + 95.50	1286.78	282 + 38.08	1284.31	284 + 70.64	1289.34
285 + 53.88	1286.06	282 + 30.38	1284.15	284 + 29.03	1288.90
285 + 12.26	1285.40	282 + 25.25	1283.44	283 + 87.41	1288.37
284 + 70.64	1284.82	282 + 20.12	1290.73	283 + 45.79	1287.77
284 + 29.03	1284.31	281 + 76.12	1281.01	283 + 12.46	1286.56
283 + 87.41	1283.86	281 + 75.50	1280.80	282 + 79.12	1284.87
283 + 45.79	1283.41	281 + 71.89	1281.95	282 + 62.46	1284.64
283 + 12.46	1283.87	281 + 65.46	1282.78	282 + 45.79	1284.41
282 + 79.12	1284.44	281 + 59.22	1283.34	282 + 32.98	1284.31
282 + 62.46	1284.71	281 + 50.18	1283.53	282 + 20.12	1284.12
282 + 45.79	1284.91	281 + 39.32	1283.96	282 + 09.11	1284.03
282 + 32.98	1284.58	281 + 23.85	1283.99	281 + 98.11	1283.92
282 + 20.12	1284.33	280 + 95.40	1283.56	281 + 87.10	1284.18
282 + 09.11	1284.34	280 + 63.60	1283.58	281 + 76.09	1283.55
281 + 98.11	1284.19	280 + 31.80	1283.63	281 + 59.61	1284.01
281 + 87.10	1284.22	280 + 00.00	1283.32	281 + 43.10	1284.88
281 + 76.09	1283.97			281 + 27.20	1284.43
281 + 59.61	1283.72			280 + 95.40	1283.31
281 + 43.10	1284.09			280 + 63.60	1282.80
281 + 27.20	1284.63			280 + 31.80	1283.33
280 + 95.40	1283.57			280 + 00.00	1283.28
280 + 63.60	1282.93				
280 + 31.80	1282.61				
280 + 00.00	1282.63				

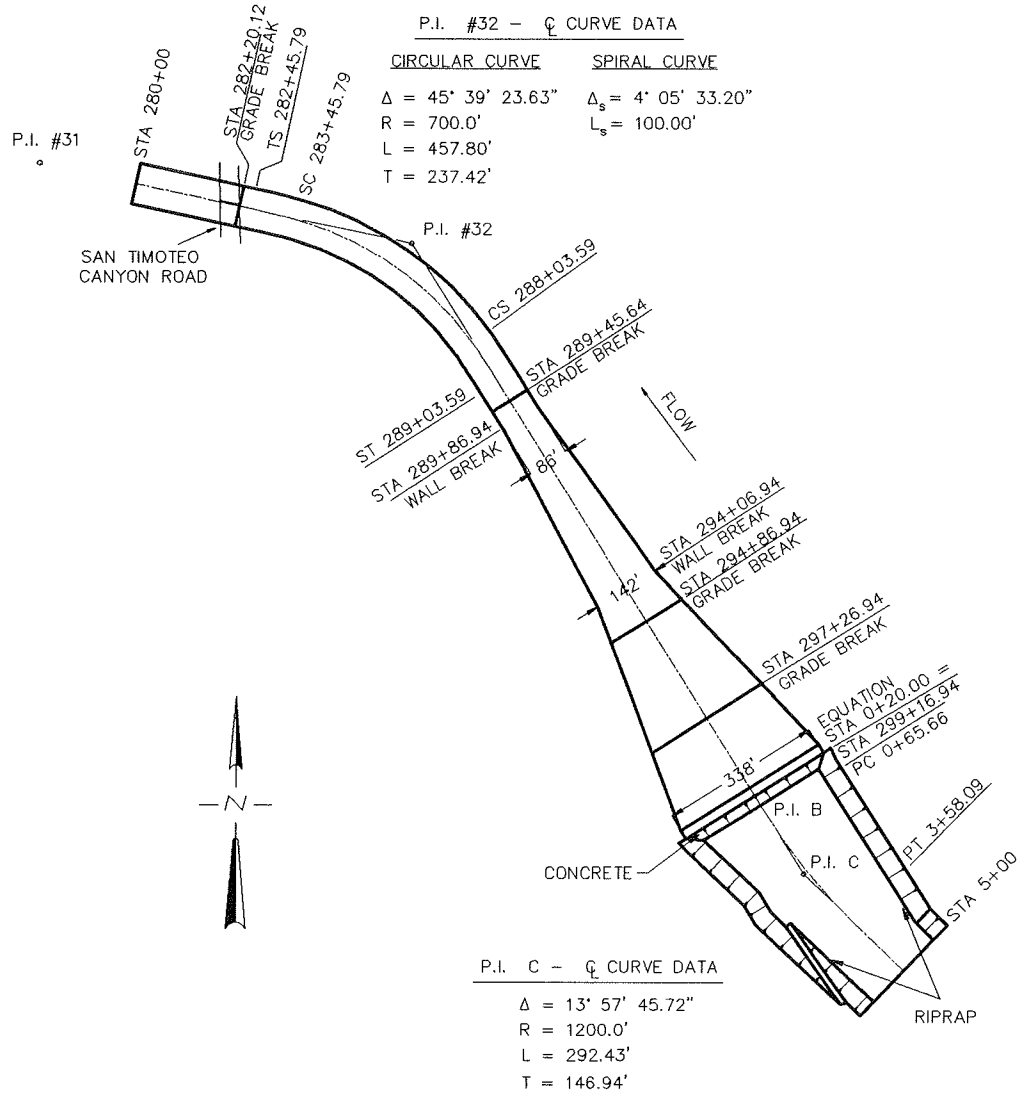

PLAN VIEW

Plate 1

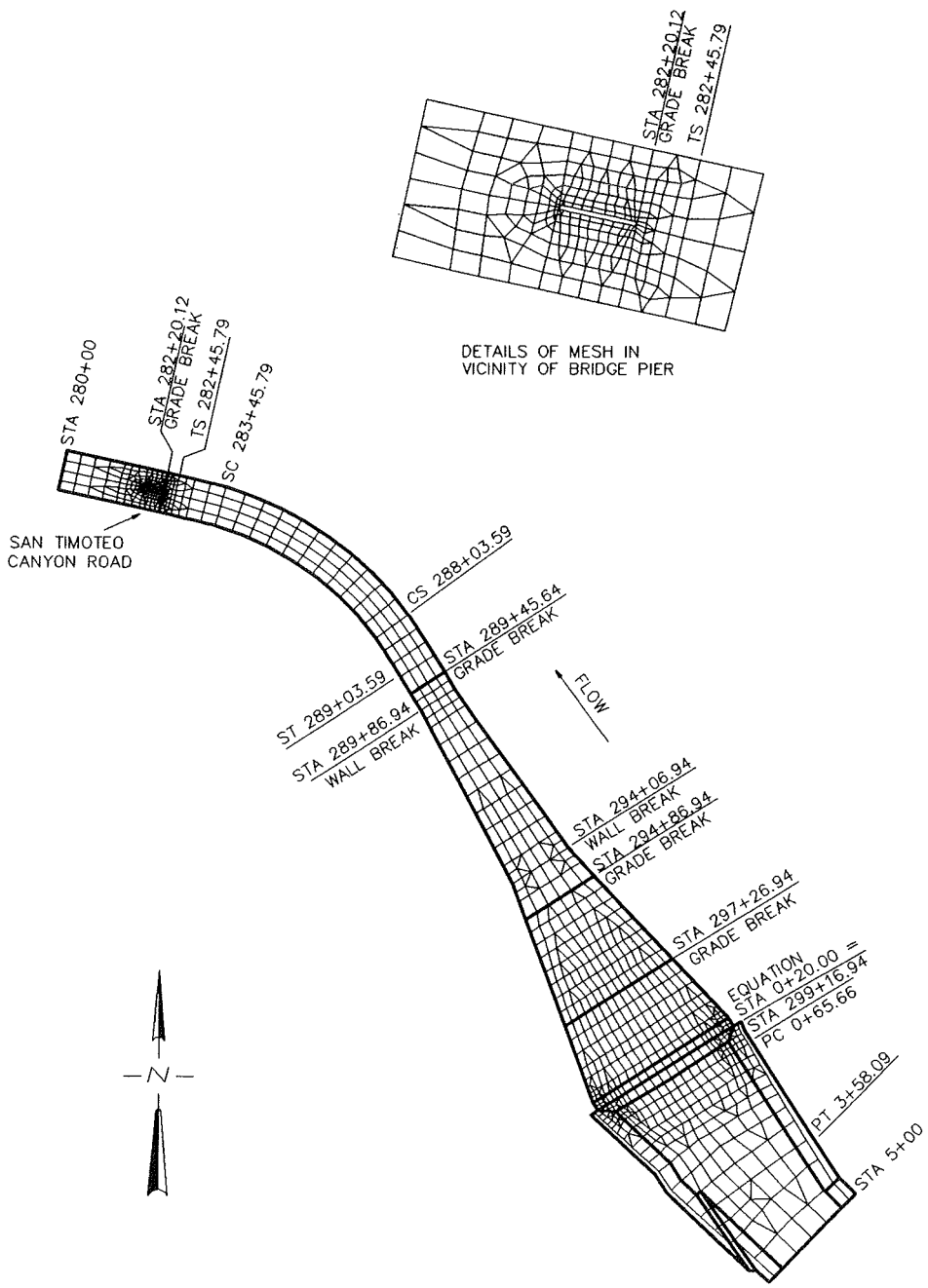

NUMERICAL MODEL
COMPUTATIONAL MESH
DISCHARGE 19,000 CFS

Plate 2

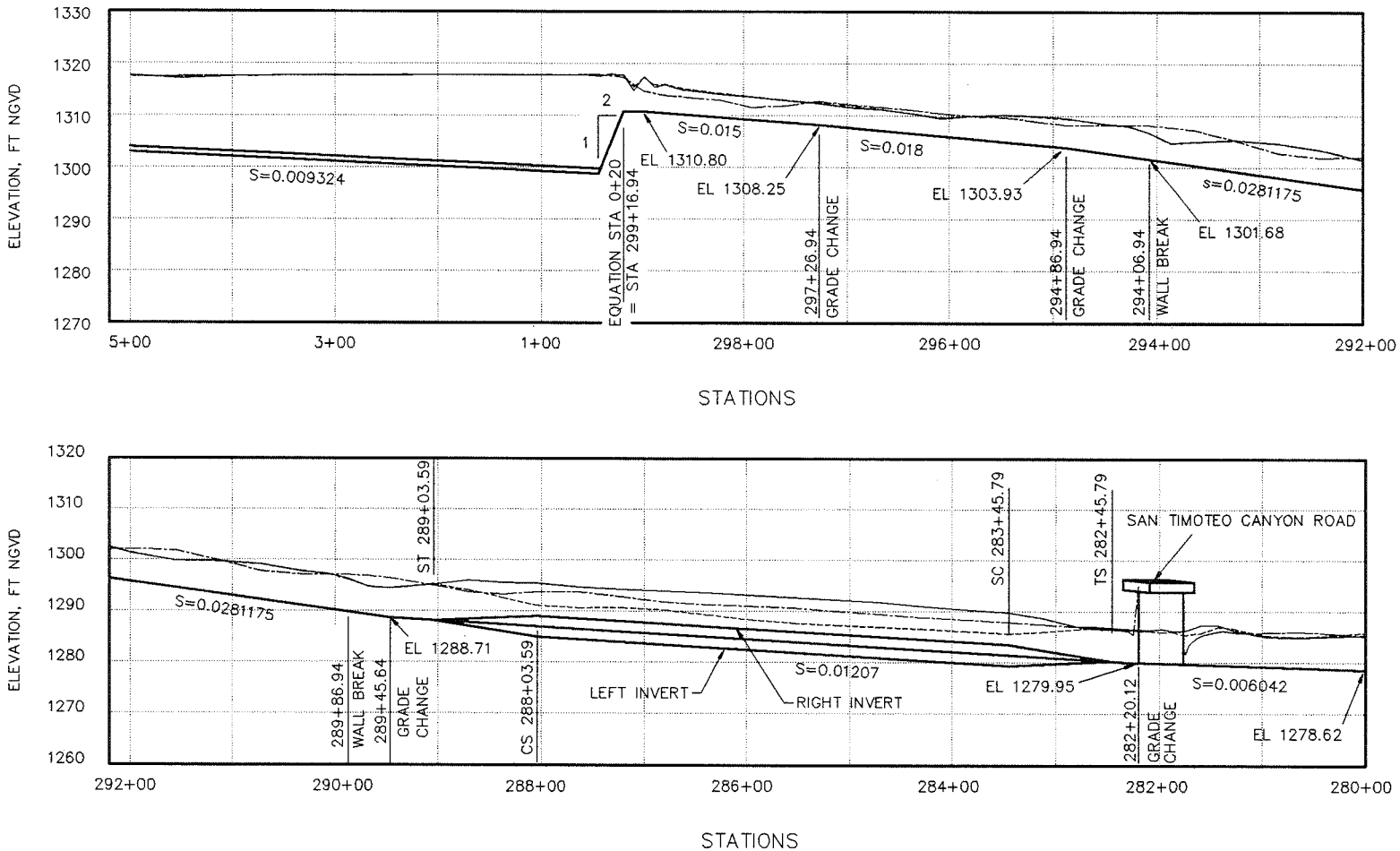

LEGEND

----- LEFT WALL
—— RIGHT WALL
—·— CENTER LINE

NOTE: THE LARGE RUNUP ON THE PIER NOSE IS MAINLY A MODEL ARTIFACT. SEE CHAPTER 4.

WATER-SURFACE PROFILES

DISCHARGE 19,000 CFS

n = 0.014

Plate 3

Plate 4

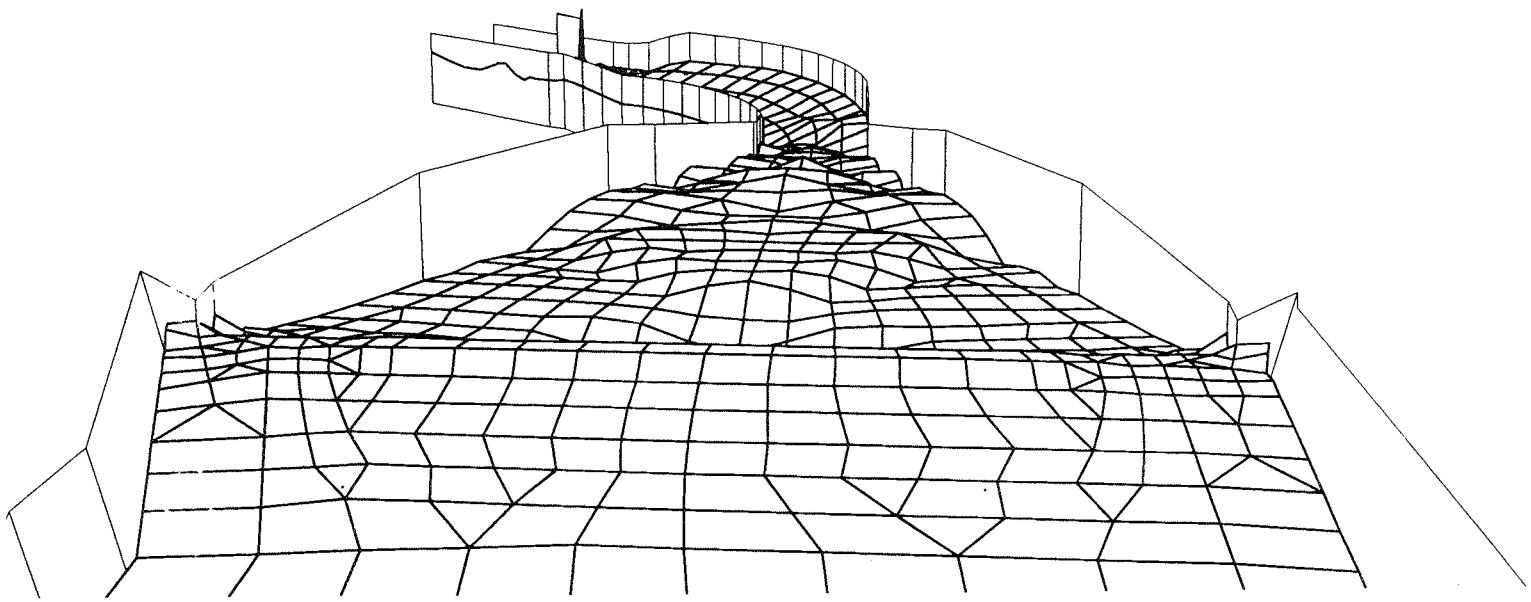

NOTE: THE LARGE RUNUP ON THE PIER
IS MAINLY A MODEL ARTIFACT.
SEE CHAPTER 4.

EXAGGERATED PERSPECTIVE OF
WATER–SURFACE MESH
LOOKING DOWNSTREAM
FROM BASIN

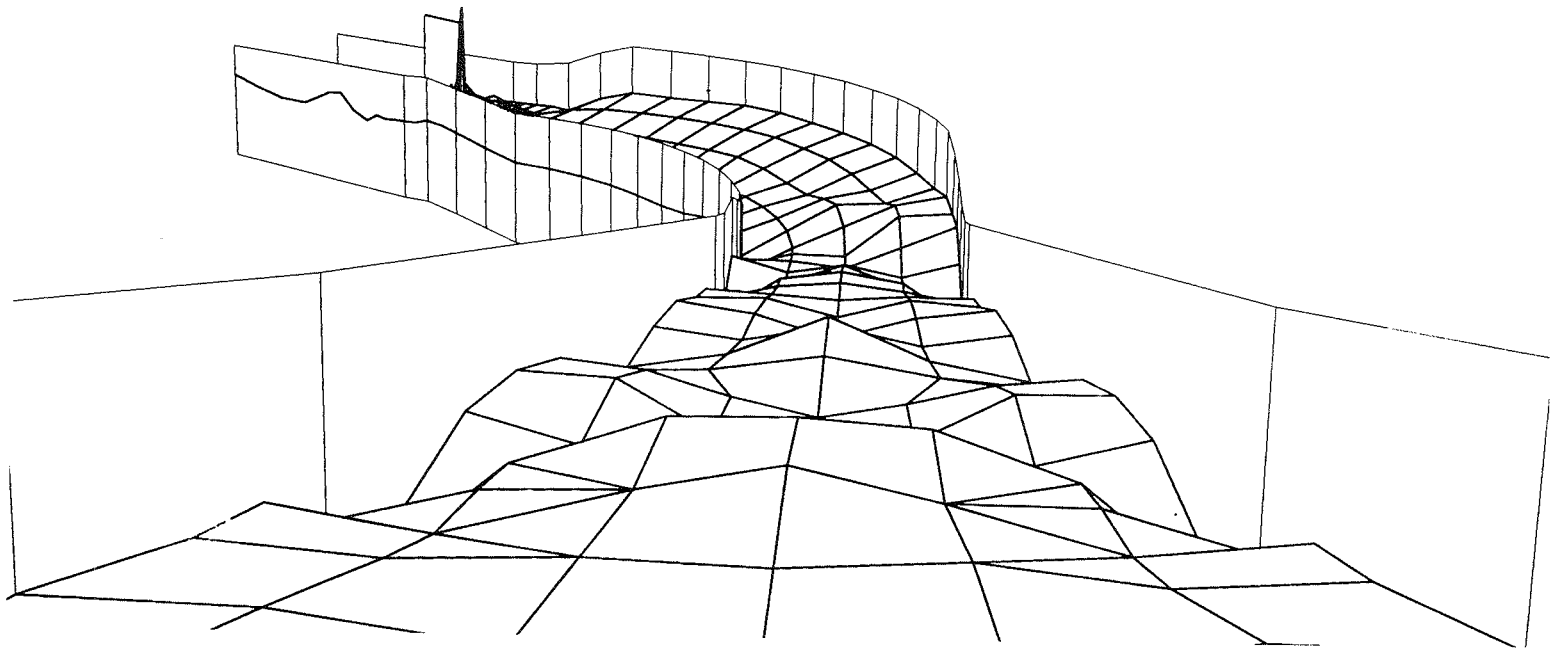

NOTE: THE LARGE RUNUP ON THE PIER
IS MAINLY A MODEL ARTIFACT.
SEE CHAPTER 4.

EXAGGERATED PERSPECTIVE OF
WATER-SURFACE MESH
LOOKING DOWNSTREAM
FROM STA 289+86.94

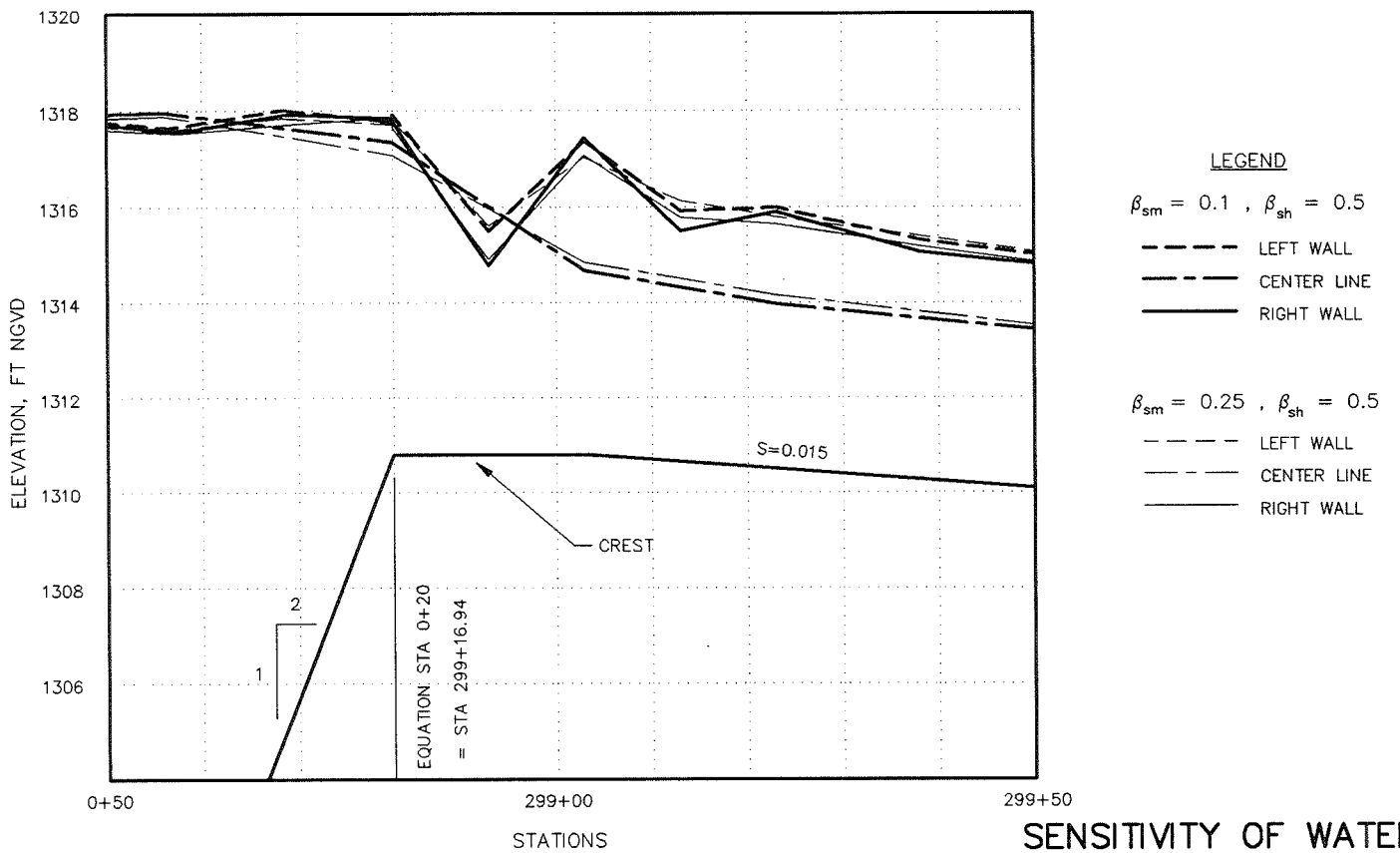

SENSITIVITY OF WATER SURFACE IN VICINITY OF CREST RELATIVE TO THE WEIGHTING COEFFICIENT, β_{sm}

DISCHARGE 19,000 CFS

n = 0.014

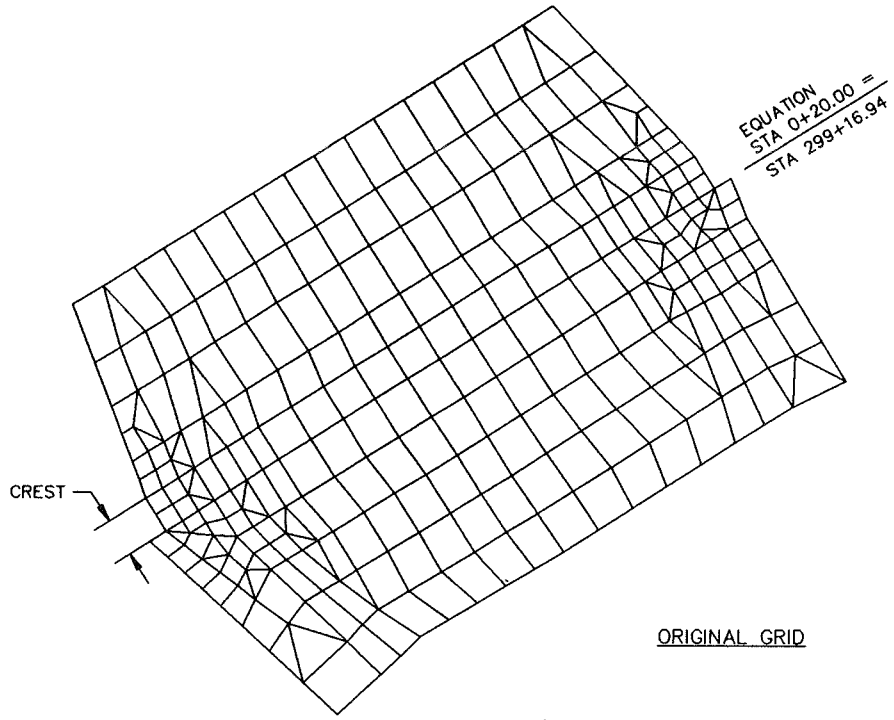

ORIGINAL GRID

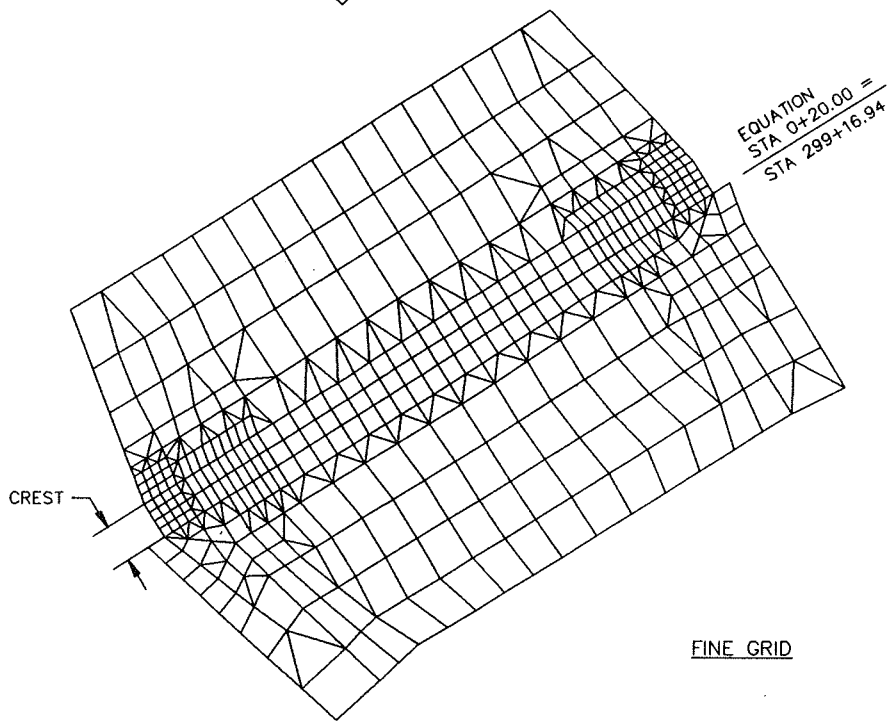

FINE GRID

ORIGINAL AND FINE MESHES
IN VICINITY OF CREST

Plate 8

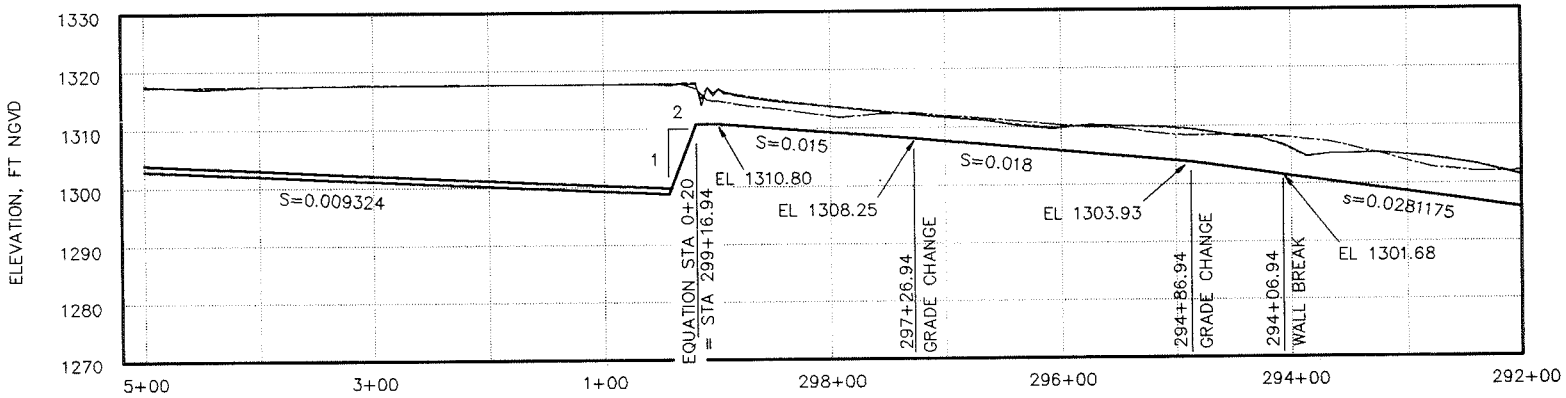

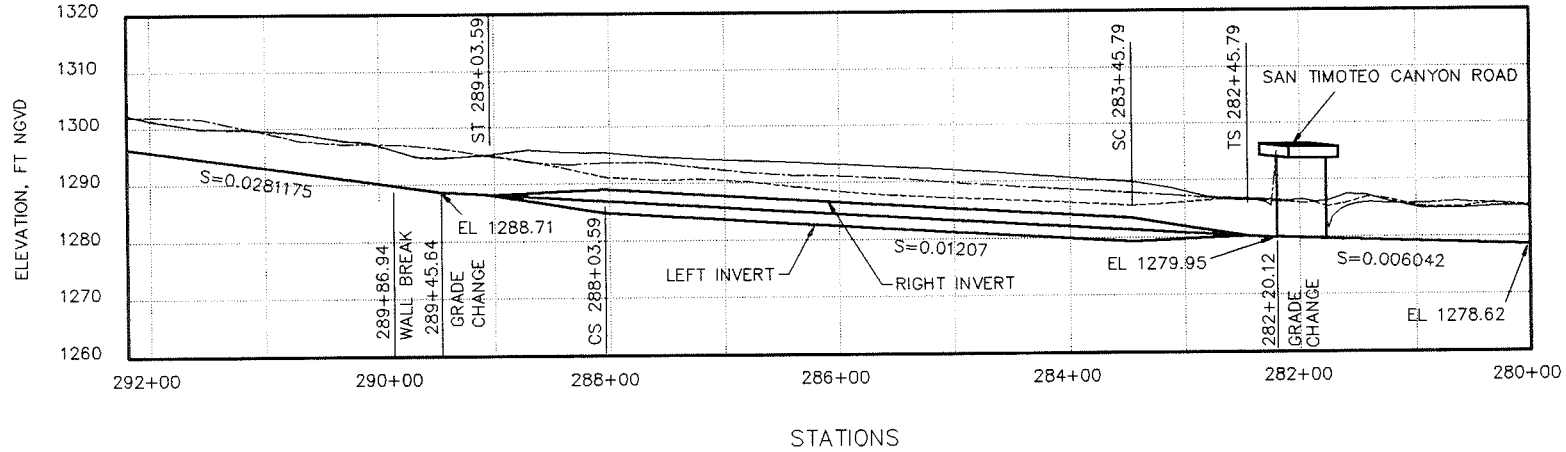

LEGEND

----- LEFT WALL
—— RIGHT WALL
—·— CENTER LINE

NOTE: THE LARGE RUNUP ON THE PIER NOSE IS MAINLY A MODEL ARTIFACT. SEE CHAPTER 4.

WATER-SURFACE PROFILES

DISCHARGE 19,000 CFS
n = 0.014
FINE GRID

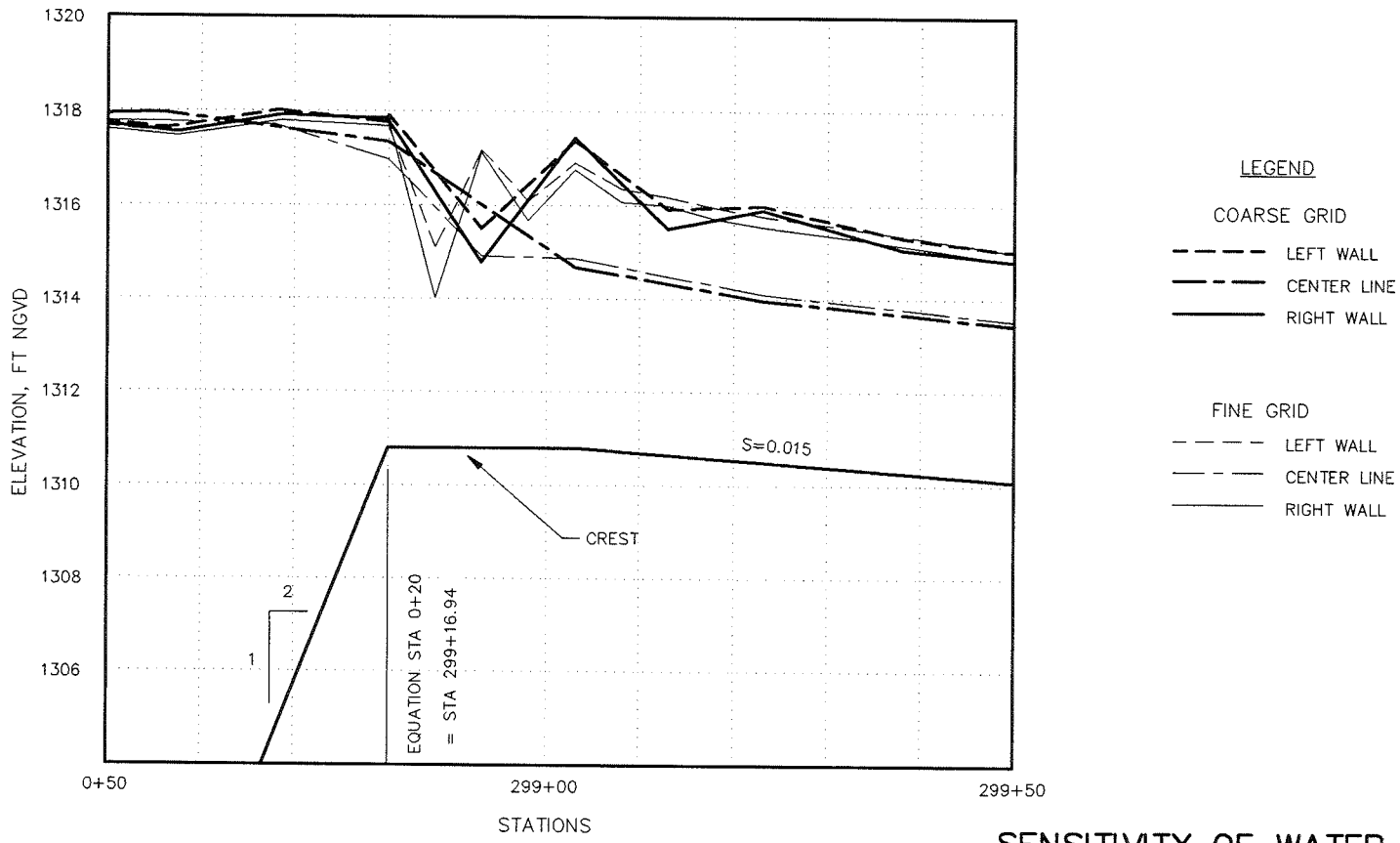

SENSITIVITY OF WATER SURFACE
IN VICINITY OF CREST
RELATIVE TO GRID RESOLUTION

DISCHARGE 19,000 CFS

n = 0.014

Plate 10

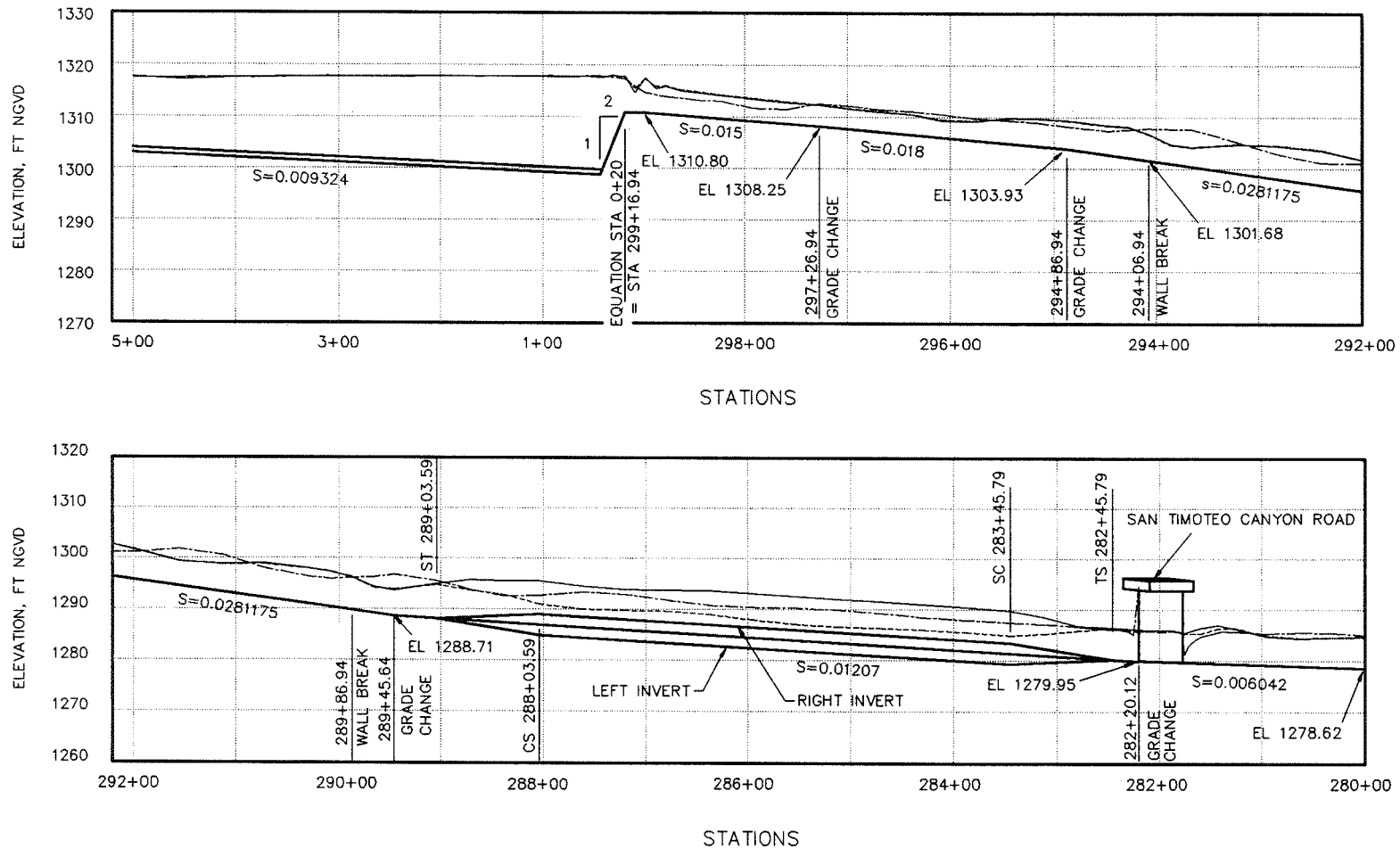

LEGEND

----- LEFT WALL
—— RIGHT WALL
—·— CENTER LINE

NOTE: THE LARGE RUNUP ON THE PIER NOSE IS MAINLY A MODEL ARTIFACT. SEE CHAPTER 4.

WATER–SURFACE PROFILES

DISCHARGE 19,000 CFS

n = 0.012

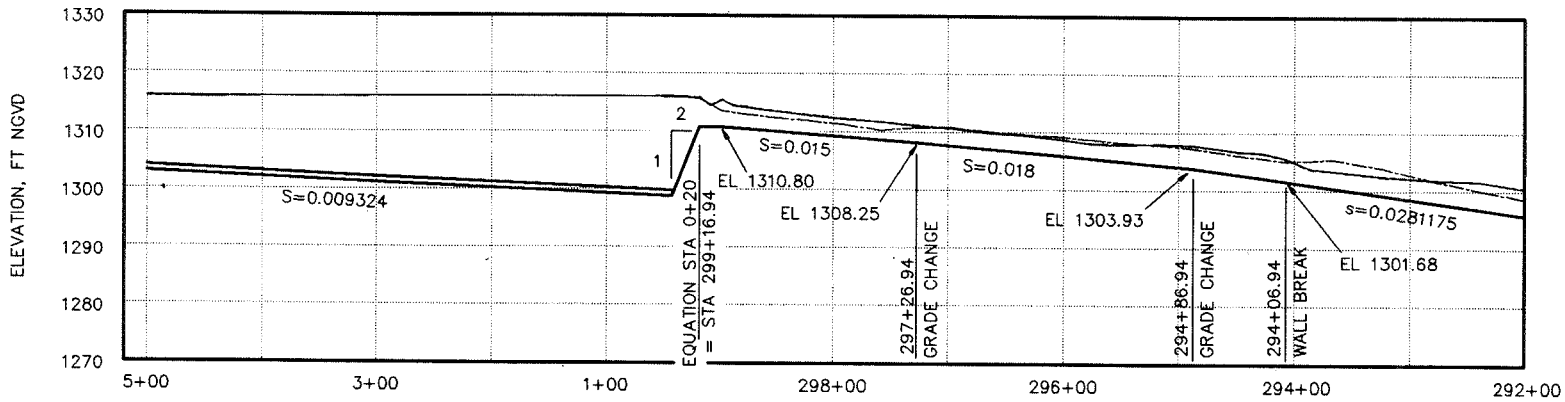

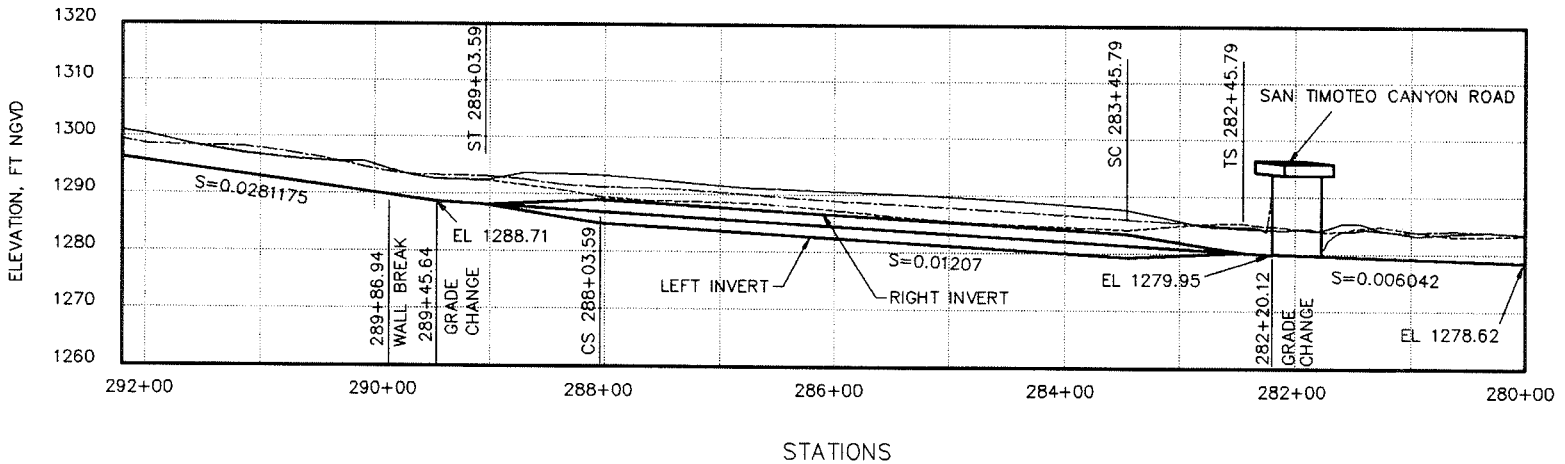

LEGEND

----- LEFT WALL
—— RIGHT WALL
—·— CENTER LINE

NOTE: THE LARGE RUNUP ON THE PIER NOSE IS MAINLY A MODEL ARTIFACT. SEE CHAPTER 4.

WATER-SURFACE PROFILES

DISCHARGE 12,000 CFS

n=0.014

Plate 11

Plate 12

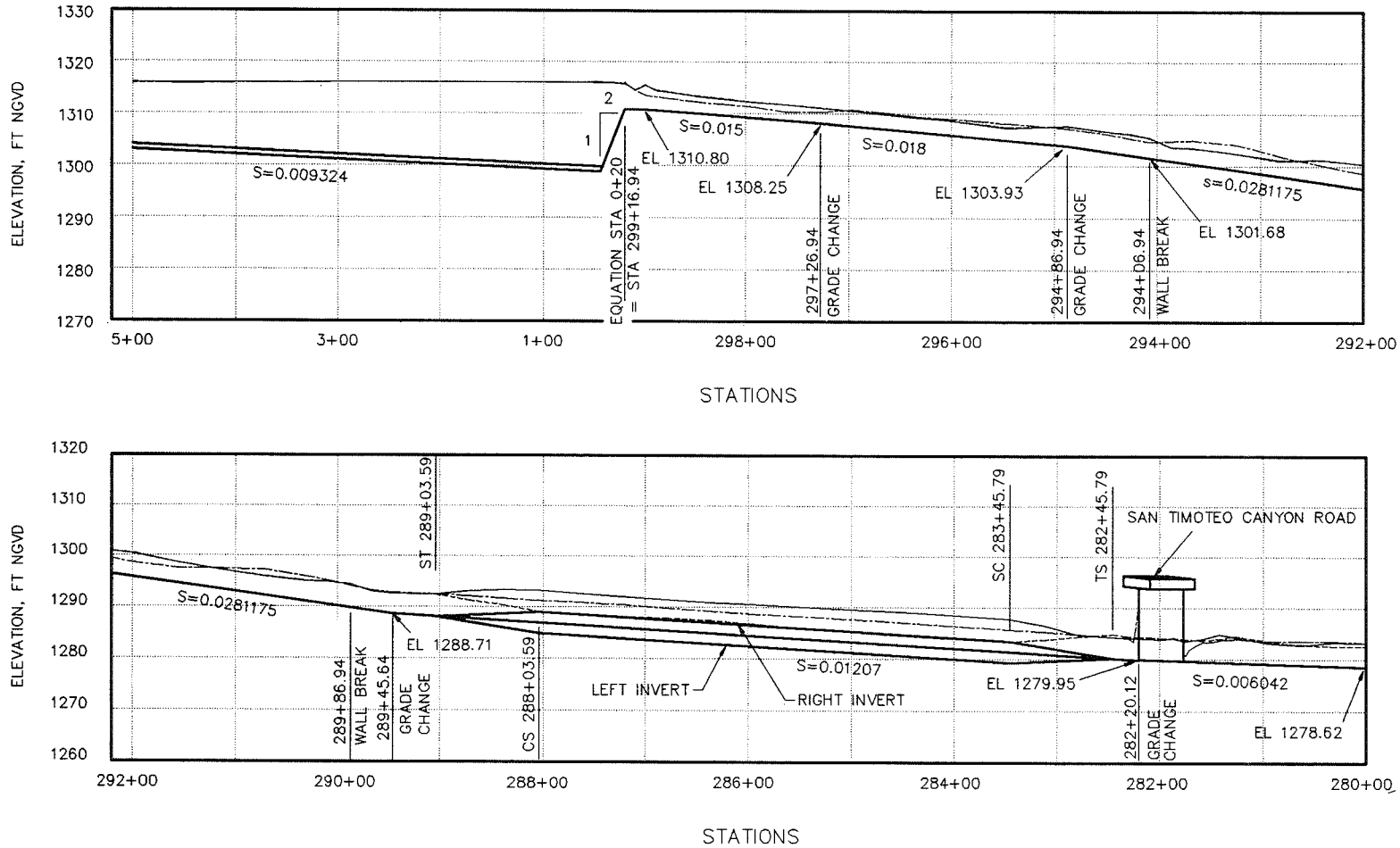

LEGEND

----- LEFT WALL
—— RIGHT WALL
—·— CENTER LINE

NOTE: THE LARGE RUNUP ON THE PIER NOSE IS MAINLY A MODEL ARTIFACT. SEE CHAPTER 4.

WATER-SURFACE PROFILES

DISCHARGE 12,000 CFS

n=0.012

Appendix A
The Hydrodynamic Model: HIVEL2D

HIVEL2D is designed to simulate flow typical in high-velocity channels. The model is a finite element description of the two-dimensional shallow-water equations in conservative form. The model does not include Coriolis, boundary, or wind effects as these are typically not important in high-velocity channels.

Vertical integration of the equations of mass and momentum conservation for incompressible flow with the assumption that vertical accelerations are negligible compared to horizontal motions and the acceleration of gravity results in the governing equations commonly referred to as the shallow-water equations. The dependent variables of the two-dimensional fluid motion are defined by the flow depth h, the x-direction component of unit discharge p, and the y-direction component of unit discharge q. These variables are functions of the independent variables x and y, the two space directions, and time t. Neglecting free-surface stresses and the effects of Coriolis force as these are not considered important in high-velocity channels, the shallow-water equations in conservative form are given as (Abbott 1979)[1]:

$$\frac{\partial \boldsymbol{Q}}{\partial t} + \frac{\partial \boldsymbol{F}_x}{\partial x} + \frac{\partial \boldsymbol{F}_y}{\partial y} + \boldsymbol{H} = \boldsymbol{0} \tag{A1}$$

where

$$\boldsymbol{Q} = \begin{bmatrix} h \\ p \\ q \end{bmatrix} \tag{A2}$$

[1] References cited in this Appendix are included in the References at the end of the main text.

$$F_x = \begin{bmatrix} p \\ \frac{p^2}{h} + \frac{1}{2}gh^2 - \frac{h\sigma_{xx}}{\rho} \\ \frac{pq}{h} - \frac{h\sigma_{yx}}{\rho} \end{bmatrix} \tag{A3}$$

$$F_y = \begin{bmatrix} q \\ \frac{pq}{h} - \frac{h\sigma_{xy}}{\rho} \\ \frac{q^2}{h} + \frac{1}{2}gh^2 - \frac{h\sigma_{yy}}{\rho} \end{bmatrix} \tag{A4}$$

$$H = \begin{bmatrix} 0 \\ gh\frac{\partial z_o}{\partial x} - g\frac{n^2 p\sqrt{p^2+q^2}}{C_0^2 h^{7/3}} \\ gh\frac{\partial z_o}{\partial y} - g\frac{n^2 q\sqrt{p^2+q^2}}{C_0^2 h^{7/3}} \end{bmatrix} \tag{A5}$$

where

p = uh, u being the depth-averaged x-direction component of velocity

q = vh, v being the depth-averaged y-direction component of velocity

g = acceleration due to gravity

$\sigma_{xx}, \sigma_{xy}, \sigma_{yx}, \sigma_{yy}$ = Reynolds stresses per unit mass where the first subscript indicates the direction and the second indicates the face on which the stress acts

ρ = fluid density

z_o = channel invert elevation

n = Manning's roughness coefficient

C_0 = dimensional constant (C_0 = 1 for SI units and C_0 = 1.486 for non-SI units)

The individual terms in the conservation equations are as follows:

a. Acceleration force per unit width:

$$\rho\frac{p^2}{h}\ ,\ \rho\frac{pq}{h}\ ,\ \rho\frac{q^2}{h}$$

b. Pressure force per unit width:

$$\frac{1}{2}\rho g h^2$$

c. Body forces per unit area:

$$\rho g h\frac{\partial z_0}{\partial x}\ ,\ \rho g h\frac{\partial z_0}{\partial y}$$

d. Bed shear stresses:

$$\rho g\frac{n^2 p\sqrt{p^2 + q^2}}{C_0^2 h^{7/3}}\ \ and\ \ \rho g\frac{n^2 q\sqrt{p^2 + q^2}}{C_0^2 h^{7/3}}$$

The Reynolds stresses are determined using the Boussinesq approach of gradient-diffusion:

$$\begin{aligned} \sigma_{xx} &= 2\nu_t\frac{\partial u}{\partial x} \\ \sigma_{xy} = \sigma_{yx} &= \nu_t\left(\frac{\partial u}{\partial y} + \frac{\partial v}{\partial x}\right) \\ \sigma_{yy} &= 2\nu_t\frac{\partial v}{\partial y} \end{aligned} \qquad \text{(A6)}$$

where ν_t is the eddy viscosity, which varies spatially and is solved empirically as a function of local flow variables (Rodi 1980).

$$\nu_t = C_b n\sqrt{8g}\, h^{5/6}\sqrt{p^2+q^2} \tag{A7}$$

where C_b is a coefficient that varies between 0.1 and 1.0.

This system of partial differential equations is solved using the finite element method. The finite element approach taken is a Petrov-Galerkin formulation that incorporates a combination of the Galerkin test function and a non-Galerkin component to control oscillations due to convection. An integration by parts procedure is used to develop the weak form of the equations. The weak form facilitates the specification of boundary conditions. The weak form is given as:

$$\sum_e \left[\int_{\Omega_e} \left(\psi_i \frac{\partial \boldsymbol{Q}}{\partial t} - \frac{\partial \phi_i}{\partial x}\boldsymbol{F}_x - \frac{\partial \phi_i}{\partial y}\boldsymbol{F}_y + \varphi_i \boldsymbol{A}\frac{\partial \boldsymbol{Q}}{\partial x} + \varphi_i \boldsymbol{B}\frac{\partial \boldsymbol{Q}}{\partial y} + \psi_i \boldsymbol{H} \right) d\Omega_e + \oint_{\Gamma_e} \phi_i \left(\boldsymbol{F}_x n_x + \boldsymbol{F}_y n_y\right) \right] = 0 \tag{A8}$$

where the variables are understood to be discrete values and

e = subscript indicating a particular element

Ω = domain

$\psi_i = \phi_i \boldsymbol{I} + \varphi_i$ = test function

ϕ_i = Galerkin part of the test function

$\boldsymbol{I}$ = identity matrix

φ_i = non-Galerkin part of the test function

$(n_x, n_y) = \hat{\boldsymbol{n}}$ = unit vector outward normal to the boundary Γ_e

and

$$\boldsymbol{A} \equiv \frac{\partial \boldsymbol{F}_x}{\partial \boldsymbol{Q}} \qquad \boldsymbol{B} \equiv \frac{\partial \boldsymbol{F}_y}{\partial \boldsymbol{Q}} \tag{A9}$$

Natural boundary conditions are applied to the sidewall boundaries through the weak statement. The sidewall boundaries are "no-flux" boundaries; that is, there is no net flux of mass or momentum through these boundaries. These boundary conditions are enforced through the line integral in the weak statement.

Petrov-Galerkin Test Function

The Petrov-Galerkin test function ψ_i, is defined (Berger 1993) as:

$$\psi_i = \phi_i \boldsymbol{I} + \varphi_i \tag{A10}$$

where

$$\varphi_i = \beta \left[\Delta x \frac{\partial \phi_i}{\partial x} \hat{\boldsymbol{A}} + \Delta y \frac{\partial \phi_i}{\partial y} \hat{\boldsymbol{B}} \right] \tag{A11}$$

where β is a dissipation coefficient varying in value from 0 to 0.5, ϕ is the linear basis function, and Δx and Δy are the grid intervals. A detailed explanation of this particular test function, in particular $\hat{A}$ and $\hat{B}$, is given in Berger (1993).

Shock Capturing

Because a lower value of β ($\beta = \beta_{SM}$) is more precise, a large value of β ($\beta = \beta_{SH} = 0.5$ where β_{SM} and β_{SH} are the Petrov-Galerkin parameters for smooth flow and for shocks) is applied only in regions in which it is needed. HIVEL2D employs a mechanism that detects shocks and increases β automatically. Therefore, β_{SH} is implemented only when needed as determined by evaluation of the element energy deviation. In a similar manner, the eddy viscosity coefficient C varies from C_{SM} to C_{SH}, the effect being that eddy viscosity is increased only in areas of greatest element energy deviation.

Temporal Derivatives

A finite difference expression is used for the temporal derivatives. The general expression for the temporal derivative of a variable, $\boldsymbol{Q}_j$, is:

$$\left[\frac{\partial \boldsymbol{Q}_j}{\partial t} \right]^{m+1} \approx \alpha \left[\frac{\boldsymbol{Q}_j^{m+1} - \boldsymbol{Q}_j^{m}}{t^{m+1} - t^{m}} \right] + (1 - \alpha) \left[\frac{\boldsymbol{Q}_j^{m} - \boldsymbol{Q}_j^{m-1}}{t^{m} - t^{m-1}} \right] \tag{A12}$$

where j is the nodal location and m is the time-step. An α equal to 1 results in a first-order backward difference approximation, and an α equal to 1.5 results in a second-order backward difference approximation of the temporal derivative.

Solution of the Nonlinear Equations

The system of nonlinear equations is solved using the Newton-Raphson iterative method. Let $\boldsymbol{R}_i$ be a vector of the nonlinear equations computed using a particular test function ψ_i and using an assumed value of $\boldsymbol{Q}_j$. $\boldsymbol{R}_i$ is the residual error for a particular test function i. Subsequently, $\boldsymbol{R}_i$ is forced toward zero as:

$$\frac{\partial \boldsymbol{R}_i^k}{\partial \boldsymbol{Q}_j^k} \Delta \boldsymbol{q}_j^k = -\boldsymbol{R}_i^k \tag{A13}$$

where the derivatives composing the Jacobian are determined analytically. This system of equations is solved for $\Delta \boldsymbol{q}_j^k$ and then an improved estimate for $\boldsymbol{Q}_j^{k+1}$ is obtained from:

$$\boldsymbol{Q}_j^{k+1} = \boldsymbol{Q}_j^k + \Delta \boldsymbol{q}_j^k \tag{A14}$$

where k is the iteration number. This procedure is continued until convergence to an acceptable residual error is obtained.

REPORT DOCUMENTATION PAGE

Form Approved
OMB No. 0704-0188

Public reporting burden for this collection of information is estimated to average 1 hour per response, including the time for reviewing instructions, searching existing data sources, gathering and maintaining the data needed, and completing and reviewing the collection of information. Send comments regarding this burden estimate or any other aspect of this collection of information, including suggestions for reducing this burden, to Washington Headquarters Services, Directorate for Information Operations and Reports, 1215 Jefferson Davis Highway, Suite 1204, Arlington, VA 22202-4302, and to the Office of Management and Budget, Paperwork Reduction Project (0704-0188), Washington, DC 20503.

1. AGENCY USE ONLY *(Leave blank)*

2. REPORT DATE
October 1994

3. REPORT TYPE AND DATES COVERED
Final report

4. TITLE AND SUBTITLE

Application of a Two-Dimensional Model of Hydrodynamics to San Timoteo Creek Flood-Control Channel, California

5. FUNDING NUMBERS

6. AUTHOR(S)

Richard L. Stockstill

7. PERFORMING ORGANIZATION NAME(S) AND ADDRESS(ES)

U.S. Army Engineer Waterways Experiment Station
3909 Halls Ferry Road, Vicksburg, MS 39180-6199

8. PERFORMING ORGANIZATION REPORT NUMBER

Miscellaneous Paper
HL-94-7

9. SPONSORING/MONITORING AGENCY NAME(S) AND ADDRESS(ES)

U.S. Army Engineer District, Los Angeles
P.O. Box 2711
Los Angeles, CA 90053-2325

10. SPONSORING/MONITORING AGENCY REPORT NUMBER

11. SUPPLEMENTARY NOTES

Available from National Technical Information Service, 5285 Port Royal Road, Springfield, VA 22161.

12a. DISTRIBUTION/AVAILABILITY STATEMENT

Approved for public release; distribution is unlimited.

12b. DISTRIBUTION CODE

13. ABSTRACT *(Maximum 200 words)*

The San Timoteo Creek, located in southern California, is a tributary of the Santa Ana River and drains portions of the San Bernardino and Riverside Counties. The existing creek has the capacity to protect the surrounding community from approximately a 20-year-frequency flood. The proposed channel improvements will provide a 100-year level of protection. The proposed channel design within the reach studied includes a sediment basin, a concrete weir followed by a converging sidewall chute, a compound horizontal curve, and a bridge pier. This study was initiated because there was concern as to the adequacy of a one-dimensional analysis of the flow conditions within the channel chute. A two-dimensional analysis was deemed necessary to evaluate the chute's influence on the flow conditions in the curve and the curve's impact on the flow conditions at the bridge.

The two-dimensional, depth-averaged flow model, HIVEL2D, was used to simulate the flows in the high-velocity channel. This model was chosen because of its ability to simulate supercritical flow and capture shocks such as oblique standing waves. Simulation results indicated that the proposed San Timoteo Channel design and in particular, the San Timoteo Canyon Road bridge, will convey the design discharge (100-year-frequency event, 19,000 cfs) in an acceptable manner.

14. SUBJECT TERMS

Finite element	San Timoteo Creek, California
Flood-control channels	Shallow-water equations
Numerical models	Two-dimensional

15. NUMBER OF PAGES
49

16. PRICE CODE

17. SECURITY CLASSIFICATION OF REPORT	18. SECURITY CLASSIFICATION OF THIS PAGE	19. SECURITY CLASSIFICATION OF ABSTRACT	20. LIMITATION OF ABSTRACT
UNCLASSIFIED	UNCLASSIFIED		